nature microbiology

Article

https://doi.org/10.1038/s41564-024-01902-8

Free fatty acid receptor 4 modulates dietary sugar preference via the gut microbiota

Received: 6 February 2024

Accepted: 5 December 2024

Published online: 13 January 2025

Check for updates

Tingting Zhang[1,2,3,8], Wei Wang[1,4,8], Jiayu Li[1,2,3], Xianlong Ye[5], Zhe Wang[1], Siyuan Cui[6], Shiwei Shen[6], Xinmiao Liang[7] ✉, Yong Q. Chen[1,2,3] ✉ & Shenglong Zhu[1] ✉

Sugar preference is a key contributor to the overconsumption of sugar and the concomitant increase in the incidence of diabetes. However, the exact mechanism of its development remains ambiguous. Here we show that the expression of free fatty acid receptor Ffar4, a receptor for long-chain fatty acids, is decreased in patients and mouse models with diabetes, which is associated with high sugar intake. Deletion of intestinal Ffar4 in mice resulted in reduced gut *Bacteroides vulgatus* and its metabolite pantothenate, leading to dietary sugar preference. Pantothenate promoted the secretion of GLP-1 which inhibited sugar preference by stimulating hepatic FGF21 release, which in turn regulates energy metabolism. These findings uncover a previously unappreciated role of Ffar4 in negatively regulating sugar preference and suggest *B. vulgatus*-derived pantothenate as a potential therapeutic target for diabetes.

The aetiology of diabetes remains elusive, with factors such as obesity, dietary habits, genetics and ageing collectively exacerbating disease onset[1]. High glucose intake has been considered as a potential environmental risk factor for the increased incidence rate of many non-communicable diseases, including obesity, cardiovascular disease, metabolic syndrome and type 2 diabetes (T2D)[2]. Populations in both developed and developing countries have experienced an increase in high-sugar and high-fat foods, and the formation of sugar preference is thought to be an important contributor to the overconsumption of sugar and the concomitant increase in diabetes rates[3–5]. The conscious perception of the sensory attributes of food by animals guides dietary choices, which manifest as sugar preference or fat preference[6]. Sugar preference means developing an appetite preference for sugar, and being able to remember this preference and take action on the basis of it. Sugar preference is a behaviour formed by animals linking flavour stimuli with in vivo stimuli of nutrients[7]. However, the exact pathophysiological mechanism of sugar preference formation remains unclear due to the complex interaction between neuromodulation and humoral regulation.

The human digestive tract contains complex assemblies of microorganisms that can impact host metabolism, immunity and neurobiology via metabolites and other pathways[8,9]. It has been hypothesized that an aberrant gut microbiota may be involved in the dietary preference behaviour[10]. Mice lacking gut microbiota showed upregulation of type 1 taste receptor 3 and sodium glucose transporter 1 expression, as well as increased sucrose intake[11]. The gut microbiota and prebiotics can also regulate host food intake[10,12], and this may include the gut–microbiota–brain axis, which can affect brain functions including the regulation of appetite, behaviour and emotions[13,14]. The gut microbiota may serve as the connection point of the gut–brain axis, thus representing a potential target in diabetes intervention and sugar preference modulation.

Research has shown that the neural basis of sugar preference is the activation of specific neurons by the gut–brain axis or liver-to-brain hormonal axis[15]. Previous studies have predominantly focused on the nexus between the nervous system and dietary preferences, with scant research exploring the relationship

[1]Wuxi School of Medicine, Jiangnan University, Wuxi, China. [2]State Key Laboratory of Food Science and Resources, School of Food Science and Technology, Jiangnan University, Wuxi, China. [3]Medical Basic Research Innovation Center for Gut Microbiota and Chronic Diseases, Ministry of Education, Wuxi, China. [4]The Second Clinical Medical School, Xuzhou Medical University, Xuzhou, China. [5]Ganjiang Chinese Medicine Innovation Center, Nanchang, China. [6]Wuxi No.2 People's Hospital Affiliated to Jiangnan University, Wuxi, China. [7]Dalian Institute of Chemical Physics, Chinese Academy of Sciences, Key Laboratory of Separation Science for Analytical Chemistry, Dalian, China. [8]These authors contributed equally: Tingting Zhang, Wei Wang.
✉e-mail: liangxm@dicp.ac.cn; yqc_lab@126.com; shenglongzhu@jiangnan.edu.cn

https://doi.org/10.1038/s41564-024-01902-8

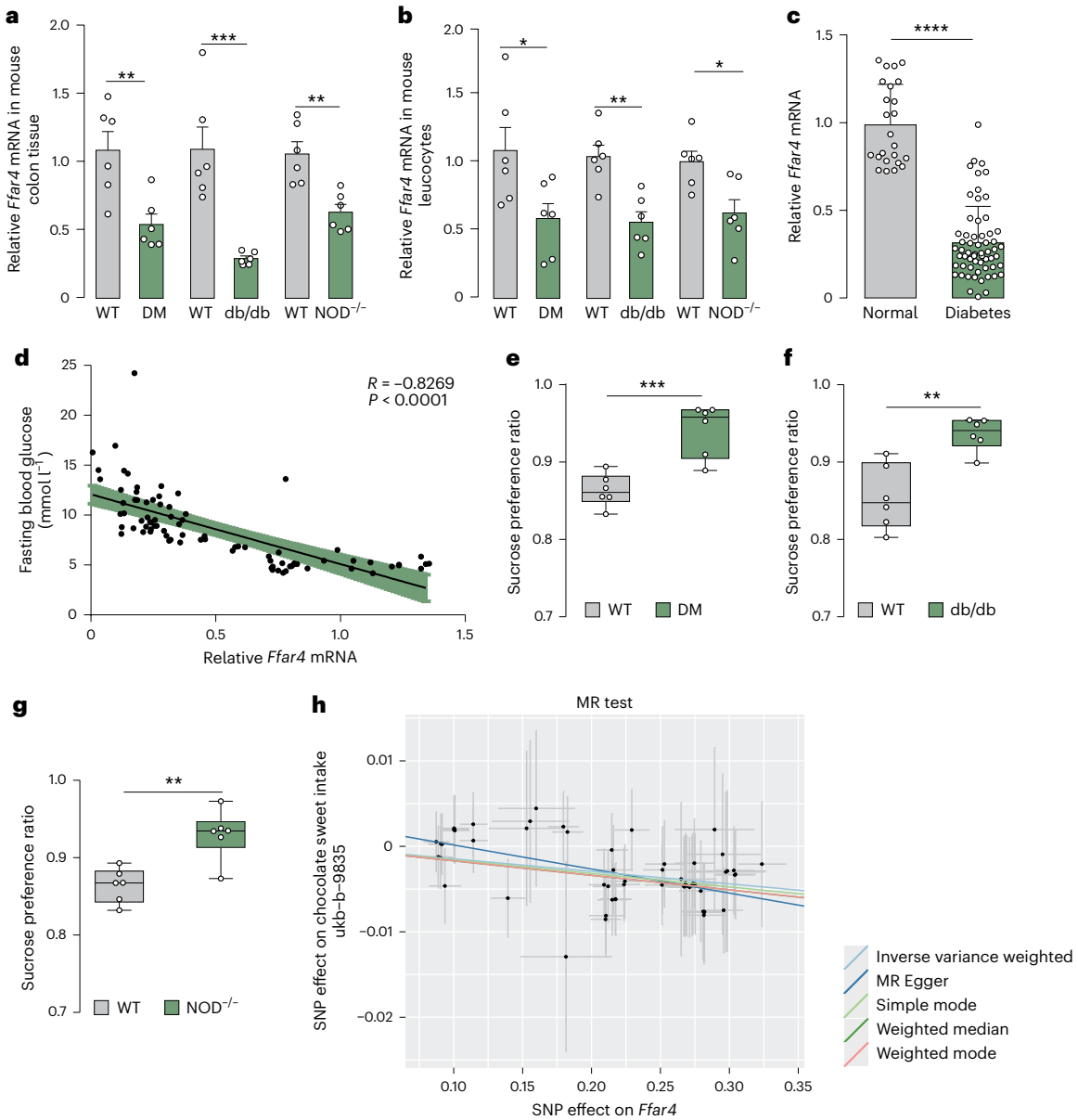

Fig. 1 | Analysis of sugar preference of diabetic mice and correlation with *Ffar4* expression. a, Expression of *Ffar4* in the colons of STZ-induced, db/db and NOD$^{-/-}$ DM model mice ($n = 6$). $P = 0.0057$, 95% confidence interval (CI): −0.8570, −0.1903; $P = 0.0006$, 95% confidence interval (CI): −1.121, −0.4179; $P = 0.0024$, 95% CI: −0.6375, −0.1828. **b**, *Ffar4* expression in blood leucocytes from STZ-induced, db/db and NOD$^{-/-}$ DM model mice ($n = 6$). $P = 0.0331$, 95% CI: −0.9258, −0.04773; $P = 0.00017$, 95% CI: −0.7185, −0.2230; $P = 0.0.129$, 95% CI: −0.6382, −0.09614. **c**, *Ffar4* expression in blood leucocytes from healthy controls and diabetic patients ($n = 24/60$). ****$P < 0.0001$, 95% CI: −0.7762, −0.5702. **d**, Correlation between *Ffar4* mRNA levels in blood leucocytes and FBG levels ($n = 84$). Shaded area represents 95% confidence intervals. **e**, Two-bottle preference assay with sucrose (100 mM) in STZ-induced DM model mice ($n = 6$). ***$P = 0.0007$, 95% CI: 0.04103, 0.1121. **f**, Two-bottle preference assay with sucrose (100 mM) in db/db mice ($n = 6$). **$P = 0.016$, 95% CI: 0.03773, 0.1194. **g**, Two-bottle preference assay with sucrose (100 mM) in NOD$^{-/-}$ mice ($n = 6$). **$P = 0.0021$, 95% CI: 0.02913, 0.09759. **h**, Scatterplot of the causal relationship of *Ffar4* with chocolate sweet intake. This plot was used to visualize the effect of each single nucleotide polymorphism (SNP). The horizontal axis represents the exposure effect and the vertical axis represents the outcome effect. The slopes of the lines represent the causal effect of each method. *P* values were determined using unpaired, two-tailed *t*-test. Data represent mean ± s.e.m. For data shown as 'box and whisker' plots: the box extends from the 25th to the 75th percentiles, the centre indicates the median, and whiskers indicate the minimum and maximum, with all data points shown. *$P < 0.05$, **$P < 0.01$, ***$P < 0.001$, ****$P < 0.0001$.

between the intestinal microenvironment and dietary preferences. The alteration in dietary preference may stem from a multifaceted interplay between genetic factors and environmental influences, with free fatty acid receptors (FFARs) potentially serving as a crucial bridge between genetic and environmental factors in the regulation of dietary preference. Activation of Ffar1 and Ffar4 occurs through medium-chain and long-chain fatty acids[16]. Fatty acids, particularly long-chain fatty acids (LCFAs), are major constituents of the human diet[17].

In this study, we found that (1) *Ffar4* expression was decreased in patients with diabetes and mice with diabetes, and *Ffar4* mutations lead to increased sugar preference among populations; (2) intestinal-specific deletion of *Ffar4* promoted sugar preference, whereas intestinal-specific overexpression of *Ffar4* mitigated sugar preference; and (3) intestinal *Ffar4*, by modulating the abundance of the gut bacterium *Bacteroides vulgatus* and employing its metabolite pantothenate, orchestrated the secretion of GLP-1. GLP-1 stimulated the secretion of FGF21 in the liver, thereby shaping the predilection for sugar in mice.

Results

Elevated dietary sugar preference is associated with decreased *Ffar4* expression

To investigate whether Ffar4 is differentially expressed in diabetes, three different models of diabetes (db/db, Nod$^{-/-}$ and STZ-induced diabetic mice (DM)) were established (Extended Data Fig. 1a). *Ffar4* expression in the mouse colon was significantly decreased in the three mouse models, and the results of *Ffar4* expression in blood leucocytes were consistent with those in colon tissue (Fig. 1a,b). Next, *Ffar4* messenger RNA expression was determined in human peripheral blood leucocytes derived from healthy humans and diabetic patients, and the results showed that Ffar4 was significantly downregulated in diabetic patients (Fig. 1c and Supplementary Table 2). We also analysed the correlation between fasting blood glucose (FBG) and the mRNA levels of *Ffar4* in human peripheral blood leucocytes, and found that FBG content was negatively correlated the mRNA levels of *Ffar4* (Fig. 1d). To further analyse the correlation between dietary sugar preference and the development of diabetes, we examined sugar preference in diabetes models. Results showed that diabetic mice all had a higher preference for sugar than control mice (Fig. 1e–g). We further analysed the correlation between *Ffar4* level in mouse colon tissue/leucocytes and sucrose preference. Results showed that the level of *Ffar4* was negatively correlated with sucrose preference (Extended Data Fig. 1b). To investigate the relationship between Ffar4 and sugar preference in populations, we analysed the chocolate sweet intake data and sugar added to tea data (https://gwas.mrcieu.ac.uk/; ID: ukb-b-9835, ukb−b−8442), and the expression quantitative trait locus (eQTL) data of *Ffar4* and performed two-sample Mendelian randomization (MR) analysis. Results showed that *Ffar4* mutations lead to increased sugar preference among populations (Fig. 1h and Extended Data Fig. 1c,d). These results suggest that there may be an intrinsic link between Ffar4 and sugar preference in the regulation of glucose homeostasis.

Systemic *Ffar4* deletion promotes dietary sugar preference in mice

Although Ffar4 is primarily expressed in the intestine, it is also widely expressed in other tissues (Fig. 2a). To clarify whether *Ffar4* deletion affects dietary preference in mice, we constructed *Ffar4* systemic knockout mice (*Ffar4*KO) (Fig. 2b,c), and consistent with previous human studies[18], found elevated FBG in *Ffar4*KO mice (Fig. 2d). In addition, *Ffar4*KO mice displayed normal diet and water consumption (Fig. 2e,f) but had a significant preference for high-sugar diet (HSD) compared with the control group (Fig. 2g,h).

To further investigate whether the dietary preference for high sugar in *Ffar4*KO mice is related to the type of sugar or taste perception, we performed a double water bottle selection test. Results showed that *Ffar4*KO mice had a preference for sucrose, fructose, glucose and dextrin compared with wild-type (WT) mice, and no preference for the artificial sweeteners aspartame, saccharin or quinine (Fig. 2i–o). These results suggest that systemic knockout of *Ffar4* affects the preference for sugar in mice, independent of taste perception.

Gut Ffar4 negatively modulates dietary sugar preference

Ffar4 is more widely expressed, with expression in tissues such as the intestinal epithelial cells (Fig. 3a), liver and microglia in the brain predominating[19]. To further investigate which tissue sources of Ffar4 regulate sugar preference in mice, we constructed various tissue-specific knockout mice, including gut epithelial cells *Ffar4*-specific knockout (Gko) (Fig. 3b,c), liver-specific knockout (Lko) (Extended Data Fig. 2a,b) and microglia-specific knockout (Mko) (Extended Data Fig. 2k,l). Results showed that Gko mice had a significant preference for HSD compared with control fl/fl, and no significant preference for high-fat diet (HFD) (Fig. 3d,e). Lko and Mko had no significant effect on dietary preference (Extended Data Fig. 2c,m). Consistent with total *Ffar4* knockout mice, Gko mice displayed normal diet and water consumption but elevated FBG (Extended Data Fig. 3a,b).

Double water bottle selection test showed that Gko mice had a preference for sucrose, fructose, glucose and dextrin, and no preference for aspartame, saccharin and quinine compared with fl/fl mice (Fig. 3f–i and Extended Data Fig. 3c–e). Lko and Mko mice had no sugar preference compared with controls (Extended Data Fig. 2d–j, n–t). These results indicate that intestinal Ffar4 is the key to regulating dietary sugar preference and that Ffar4 signals can distinguish natural sugars from artificial sweeteners, which further verifies that this preference is not related to taste perception.

To further substantiate the role of intestinal Ffar4 in regulating sugar preference in mice, we constructed *Ffar4* intestine-specific overexpression mice (Ge) and control mice (t/w) (Fig. 3j,k). The amount of food and water consumed by Ge mice was not significantly different from that of t/w mice, but FBG was significantly lower in Ge mice than in t/w mice (Extended Data Fig. 3f,g). Dietary selection experiments showed that Ge mice had a significantly lower preference for HSD compared with the control group (Fig. 3l and Extended Data Fig. 3h). Double water bottle selection test showed that Ge mice exhibited a significantly lower preference for sucrose, fructose, glucose and dextrin, and no preference for aspartame, saccharin and quinine compared with t/w mice (Fig. 3m–p and Extended Data Fig. 3i–k).

Identification of *B. vulgatus* as the key microbe involved in Ffar4-regulated sugar preference

It has been hypothesized that an aberrant gut microbiota may be involved in food preference. We speculated that gut microbiota participated in Ffar4-mediated sugar preference. Thus, we conducted a co-housing experiment and faecal microbiota transplantation (FMT) experiment (Extended Data Fig. 4a). Results showed that the sugar preference of *Ffar4*KO and Gko mice significantly decreased after 2 months of co-housing (Fig. 4a and Extended Data Fig. 4b). In contrast, the sugar preference of Ge mice significantly increased (Fig. 4b). FMT experiment results showed that after antibiotic cocktails (ABX) treatment, the difference in sugar preference between Gko mice and fl/fl mice disappeared (Fig. 4c), and the difference in sugar preference between Ge mice and t/w mice disappeared (Fig. 4d). After FMT, the sugar preference of Gko mice significantly decreased (Fig. 4e). We also found the same results in the *Ffar4*KO and WT

Fig. 2 | Effect of systemic *Ffar4* knockout on dietary preference in mice. **a**, The expression of *Ffar4* in human organs. **b**, *Ffar4*KO mouse generation (top). Genotyping primers amplified a 110-bp band from wild-type mouse DNA and an 87-bp band from knockout mouse DNA by PCR ($n = 6$) (bottom). **c**, *Ffar4* expression in each major tissue of *Ffar4*KO mice ($n = 6$). ****$P < 0.0001$, 95% CI: −1.134, −0.7993. **d**, Fasting blood glucose of mice ($n = 6$). *$P = 0.0118$, 95% CI: 0.1511, 0.9489. **e**, Daily food intake of mice ($n = 10$). **f**, Daily water intake of mice ($n = 13$). **g**, Dietary selection assay with HSD/ND in mice ($n = 10$). ****$P < 0.0001$, 95% CI: 0.2633, 0.4539. **h**, Dietary selection assay with HFD/ND in mice ($n = 10$). **i**, Two-bottle preference assay with sucrose (100 mM) in mice ($n = 9$). ****$P < 0.0001$, 95% CI: 0.02616, 0.05579. **j**, Two-bottle preference assay with fructose (100 mM) in mice ($n = 9$). ****$P < 0.0001$. **k**, Two-bottle preference assay with glucose (100 mM) in mice ($n = 9$). ****$P < 0.0001$, 95% CI: 0.08252, 0.09829. **l**, Two-bottle preference assay with dextrin (2%) in mice ($n = 9$). ****$P < 0.0001$, 95% CI: 0.08783, 0.1253. **m**, Two-bottle preference assay with aspartame (0.2%) in mice ($n = 9$). **n**, Two-bottle preference assay with saccharin (0.2%) in mice ($n = 9$). **o**, Two-bottle preference assay with quinine (1.5 mM) in mice ($n = 6$). *P* values were determined using unpaired, two-tailed *t*-test. Data represent mean ± s.e.m. For data shown as 'box and whisker' plots: the box extends from the 25th to the 75th percentiles, the centre indicates the median, and whiskers indicate the minimum and maximum, with all data points shown.

https://doi.org/10.1038/s41564-024-01902-8

groups (Extended Data Fig. 4c,d). In contrast, the sugar preference of Ge mice significantly increased (Fig. 4f). These results indicate that the colon microbiota is involved in the alterations in sugar preference mediated by Ffar4.

To further investigate the key bacterial community involved in changes in sugar preference mediated by Ffar4, we collected faecal samples from Gko, fl/fl, Ge and t/w mice for 16S rRNA amplicon sequencing. Results showed significant differences in colon microbiota between

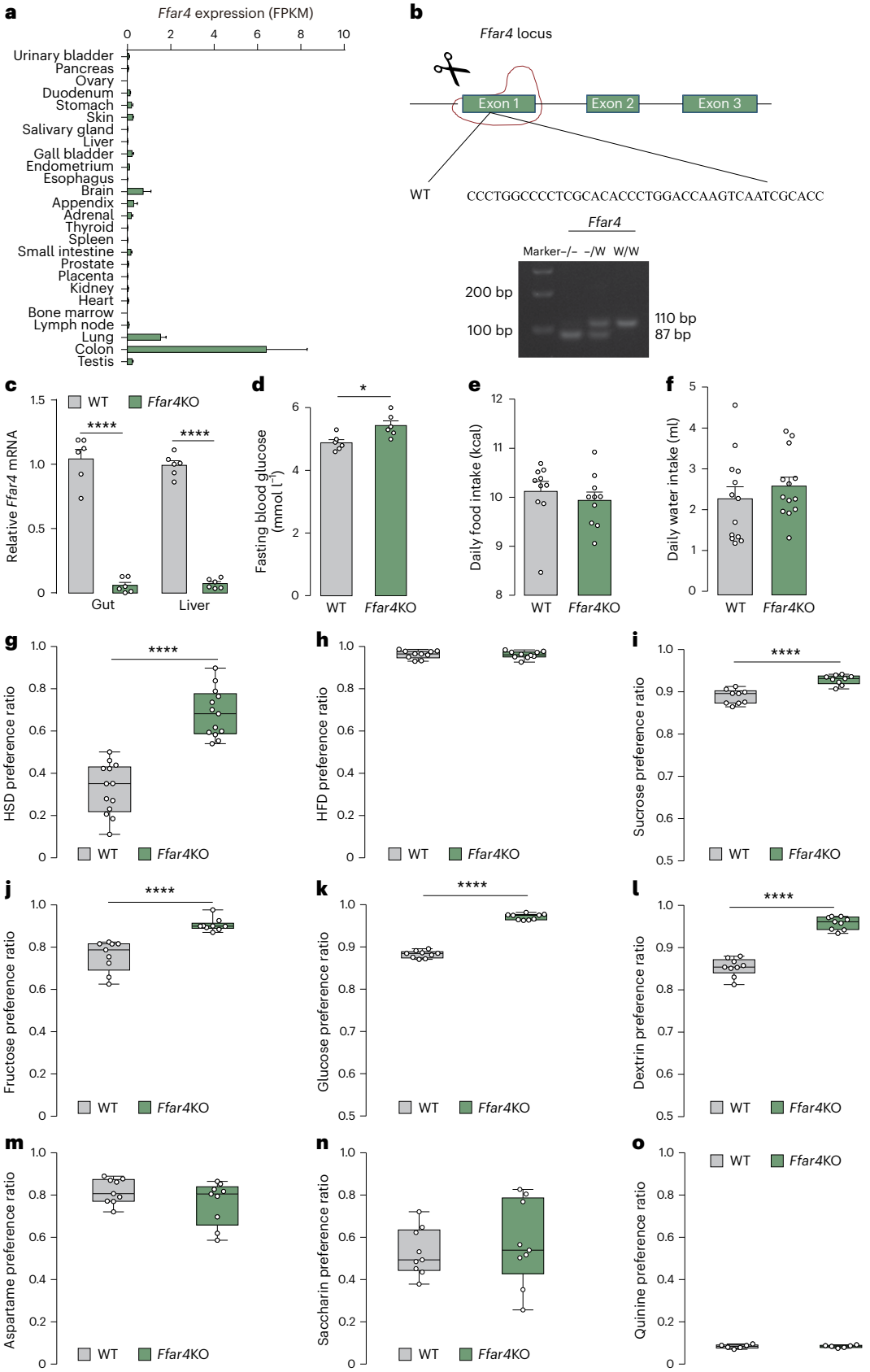

https://doi.org/10.1038/s41564-024-01902-8

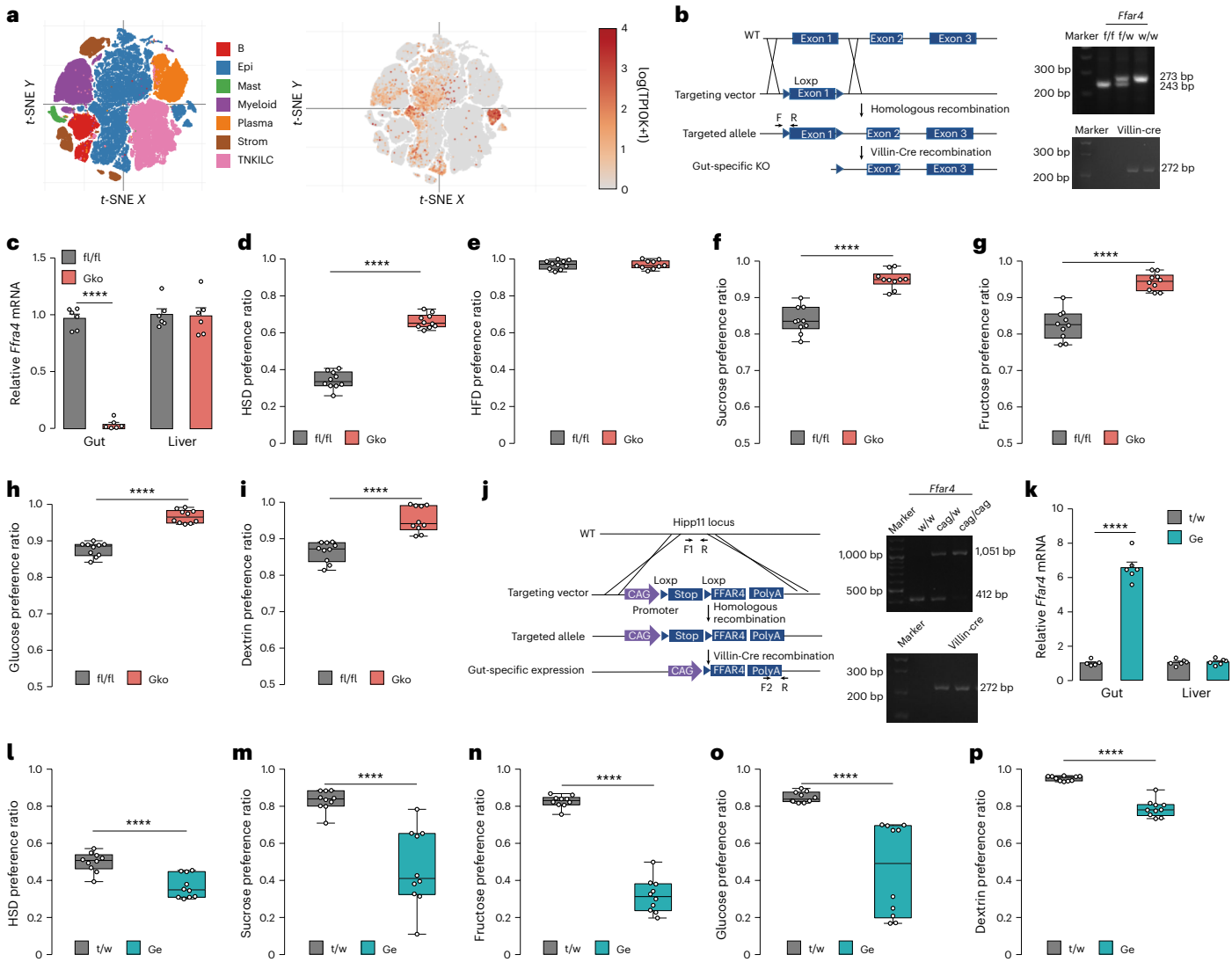

Fig. 3 | Ffar4 in the intestine negatively regulates dietary sugar preference. **a**, *T*-distributed stochastic neighbour embedding (*t*-SNE) plot of the human colon cancer atlas (visualization available at https://singlecell.broadinstitute.org/). The left panel represents all cell types; the right panel represents *Ffar4* expression in all cell types. **b**, Generation of the Gko mouse model. We constructed gut epithelial cell *Ffar4*-specific knockout mice (Villin-Cre; Ffar4Loxp/Loxp, abbreviated Gko) and corresponding control mice (Ffar4Loxp/Loxp, abbreviated as fl/fl). Genotyping primers amplified a 243-bp band from WT mouse DNA, a 273-bp band from fl/fl mouse DNA and a 272-bp band from Cre mouse DNA ($n = 6$). **c**, *Ffar4* expression in major tissues of Gko mice ($n = 6$). ****$P < 0.0001$, 95% CI: −1.004, −0.8234. **d**, Dietary selection assay with HSD/ND in mice ($n = 10$). ****$P < 0.0001$, 95% CI: 0.2766, 0.3553. **e**, Dietary selection assay with HFD/ND in mice ($n = 10$). **f**, Two-bottle preference assay with sucrose (100 mM) in mice ($n = 10$). ****$P < 0.0001$, 95% CI: 0.08319, 0.1412. **g**, Two-bottle preference assay with fructose (100 mM) in mice ($n = 10$). ****$P < 0.0001$, 95% CI: 0.08652, 0.1477. **h**, Two-bottle preference assay with glucose (100 mM) in mice ($n = 10$). ****$P < 0.0001$, 95% CI: 0.07213, 0.1069. **i**, Two-bottle preference assay with dextrin (2%) in mice ($n = 10$). ****$P < 0.0001$, 95% CI: 0.05861, 0.1178. **j**, Generation of the Ge mouse model. We constructed Ffar4 intestine-specific overexpression mice (Villin-Cre; t/w), referred to as Ge. Genotyping primers amplified a 412-bp band from wild-type mouse DNA, a 1,051-bp band from cag/cag mouse DNA and a 272-bp band from Cre mouse DNA ($n = 6$). **k**, *Ffar4* expression in major tissues of Ge mice ($n = 6$). ****$P < 0.0001$, 95% CI: 4.710, 6.168. **l**, Dietary selection assay with HSD/ND in mice ($n = 10$). ****$P < 0.0001$, 95% CI: −0.1877, −0.07898. **m**, Two-bottle preference assay with sucrose (100 mM) in mice ($n = 10$). ****$P < 0.0001$, 95% CI: −0.5130, −0.2264. **n**, Two-bottle preference assay with fructose (100 mM) in mice ($n = 10$). ****$P < 0.0001$, 95% CI: −0.5805, −0.4516. **o**, Two-bottle preference assay with glucose (100 mM) in mice ($n = 10$). ****$P < 0.0001$. **p**, Two-bottle preference assay with dextrin (2%) in mice ($n = 10$). ****$P < 0.0001$. *P* values were determined using unpaired, two-tailed *t*-test. Data represent mean ± s.e.m. For data shown as 'box and whisker' plots: the box extends from the 25th to the 75th percentiles, the centre is the median, and whiskers indicate the minimum and maximum, with all data points shown.

Ffar4 knockout or overexpression mice and control mice at multiple levels (Fig. 4g,h). A total of 6 differential bacteria at the genus level were identified to be dependent on Ffar4 expression (Fig. 4i). Then, differential bacteria (logFC > 2) were selected for the Venn analysis, which singled out *Bacteroides*. The abundance of *Bacteroides* was significantly decreased in Gko mice but significantly increased in Ge mice (Fig. 4j).

To further identify specific differentially abundant bacterial species, we quantified the common *Bacteroides* species in the Gko, fl/fl, Ge and t/w mice[20]. Results showed that *B. vulgatus* was significantly decreased in Gko mice and increased in Ge mice (Fig. 4k and Extended Data Fig. 4e,f). We also quantified the change in *B. vulgatus* in co-housed Gko or Ge or *Ffar4*KO, and found that the abundance of *B. vulgatus* in co-housed Gko and *Ffar4*KO was significantly higher than in the control group, and the abundance of *B. vulgatus* in co-housed Ge was significantly lower than in the control group (Fig. 4l and Extended Data Fig. 4g). Furthermore, we quantified the change in *B. vulgatus*

in diabetic mice and found that its abundance in diabetic mice was significantly lower than in the control group (Extended Data Fig. 4h). In addition, we collected faecal samples from 45 patients with diabetes and 15 healthy people (Supplementary Table 3), and found the faecal *B. vulgatus* abundance in patients with diabetes to be significantly lower than in the control group (Extended Data Fig. 4i).

To further verify whether *B. vulgatus* modulates sugar preference in mice, we performed reverse experiments with *B. vulgatus* and *Bacteroides dorei (B. dorei)*, which ranked as the top two in quantitative abundance. Results showed that after 10 days of gavage, *B. vulgatus or B. dorei* successfully colonized in mice gut (Extended Data Fig. 4j,k). Compared with the control group, the sugar preference of Gko mice orally gavaged with *B. vulgatus* was significantly reduced (Fig. 4m), while the sugar preference of mice orally gavaged with *B. dorei* was not significantly different from the control group (Extended Data Fig. 4l). In addition, after Gko mice were supplemented with *B. vulgatus*, FBG was significantly reduced compared with the control group (Fig. 4n). After *B. dorei* supplementation, there was no significant difference in the FBG of Gko mice compared with the control group (Extended Data Fig. 4m). Taken together, these findings indicate that gut Ffar4 regulates sugar preference by modulating the abundance of *B. vulgatus*.

Pantothenate is the key metabolite in *B. vulgatus* regulating sugar preference

The profound influence of the gut microbiota on the host is strongly associated with complex interactions comprising a series of host–microbe metabolic axes. Therefore, we conducted a high-throughput non-targeted metabolomics analysis of *B. vulgatus* in in vitro culture (Fig. 5a–c). We selected differential metabolites (logFC > 2), intersected the 0 h vs 12 h and 0 h vs 24 h groups, and found that 11 metabolites were significantly changed (Fig. 5d), with pantothenate ranking first among the metabolites (Fig. 5e,f). Interestingly, our previous study also indicated that Ffar4 deficiency regulated pantothenate in fatty liver models[21]. Therefore, we speculate that pantothenate may be the key metabolite in *B. vulgatus* regulating sugar preference, and further measured the content of pantothenate in the serum of Gko, *Ffar4*KO, Ge and the control group. Results showed that the content of pantothenate in the serum of Gko and *Ffar4*KO mice significantly decreased compared with that of the control group, while the content of pantothenate in the serum of Ge mice increased compared with that of the control group (Fig. 5g and Extended Data Fig. 5a). Co-housing experiment results showed that the content of pantothenate in co-housed Gko mice or *Ffar4*KO mice was significantly higher than in the control group, and the content of pantothenate in the co-housed Ge group was significantly lower than in the control group (Extended Data Fig. 5b,c). In addition, the expression level of *Ffar4* was positively correlated with pantothenate content (Extended Data Fig. 5d).

We measured the content of pantothenate in mouse serum after treatment with *B. vulgatus* or *B. dorei* and found the pantothenate to be significantly increased after *B. vulgatus* treatment but not after *B. dorei* treatment (Extended Data Fig. 5e). Furthermore, the pantothenate content was reduced with the aggravation of diabetes (Fig. 5h and Supplementary Table 2), and serum pantothenate content was significantly inversely correlated with triglyceride (TG) and FBG (Fig. 5i,j and Extended Data Fig. 5f–k).

Therefore, we replenished pantothenate to verify whether it affected the sugar preference of mice. Results showed that pantothenate significantly reduced sugar preference in Gko mice (Fig. 5k). We also measured the levels of pantothenate in mouse faeces and portal blood. Results showed that the pantothenate content in the faeces and portal blood of Gko mice was significantly lower than that of the control group. However, after gavaging with ABX, the difference in pantothenate content in the faeces and portal blood of Gko and control group mice was eliminated. After gavaging with pantothenate, the pantothenate content in the faeces and portal vein blood of Gko and control group mice was significantly increased (Extended Data Fig. 5l,m).

B. vulgatus and pantothenate were administered to diabetic mice and sugar preference was then tested. Results showed that *B. vulgatus* and pantothenate significantly reduced FBG in diabetic mice (Extended Data Fig. 5n). After administration with *B. vulgatus* and pantothenate, the sugar preference of diabetic mice significantly decreased (Extended Data Fig. 5o). Taken together, these results indicate that pantothenate is the key metabolite in *B. vulgatus* regulating sugar preference.

Pantothenate boosts GLP-1 secretion which inhibits sugar preference by stimulating hepatic FGF21 release

Numerous studies have shown that gut hormones play key roles in feeding behaviour, and studies have demonstrated that Ffar4 regulates the secretion of gut hormones[22,23]; thus, we analysed the correlation between pantothenate content and several key gut peptides in the serum of diabetic mice and showed that pantothenate content was positively correlated with GLP-1 (Fig. 6a); nevertheless, we found no correlation between pantothenate content and peptide YY (PYY)/glucose-dependent insulinotropic polypeptide (GIP)/cholecystokinin (CCK) content (Extended Data Fig. 6a–c). Generally similar results were observed in the serum of diabetic patients, and pantothenate content was positively correlated with GLP-1 (Fig. 6b). In addition, the intestinal hormones in Gko and control mice supplemented with *B. vulgatus* and pantothenate were also determined. Results showed that GLP-1 secretion was increased in Gko mice supplemented with *B. vulgatus* and pantothenate (Fig. 6c), while reversing *B. vulgatus* and pantothenate did not change the secretion of PYY/GIP/CCK (Extended Data Fig. 6d–f). Moreover, the GLP-1 level in the portal blood of Gko mice was significantly lower than that of the control group. After gavage with *B. vulgatus* and pantothenate, the GLP-1 in the portal vein blood of Gko mice was significantly increased (Extended Data Fig. 6g). Meanwhile, the levels of GLP-1 in diabetic mice were significantly lower than those in the control group (Extended Data Fig. 6h). Interestingly, our results showed that *B. vulgatus* and pantothenate only increased the content of GLP-1 in Gko mice, but did not affect the GLP-1 in control

Fig. 4 | Sugar preference of Gko/Ge mice after co-housing/FMT with control group, and gut microbial profiling. a, Two-bottle preference assay with sucrose (100 mM) in co-housed Gko mice ($n = 8$). ***$P < 0.001$. **b**, Two-bottle preference assay with sucrose (100 mM) in co-housed Ge mice ($n = 8$). ***$P < 0.001$. **c**, Two-bottle preference assay with sucrose (100 mM) in Gko and fl/fl mice administered ABX ($n = 8$). **d**, Two-bottle preference assay with sucrose (100 mM) in Ge and t/w mice administered ABX ($n = 8$). **e**, Two-bottle preference assay with sucrose (100 mM) in Gko and fl/fl mice after FMT ($n = 8$). ****$P < 0.0001$, 95% CI: 0.1047, 0.1748; ****$P < 0.0001$, 95% CI: −0.1384, −0.1021. **f**, Two-bottle preference assay with sucrose (100 mM) in Ge and t/w mice after FMT ($n = 8$). ***$P < 0.001$; ****$P < 0.0001$, 95% CI: 0.1461, 0.2654. **g**, Stacked plot of intestinal flora genera abundance in Gko mice vs fl/fl mice. **h**, Stacked plot of intestinal flora genera abundance in Ge mice vs t/w mice. **i**, $\log_2$FC of differential genera in Gko mice vs Ge mice. **j**, Wayne plot of differential genera in Gko mice vs Ge mice; abundance of the genus *Bacteroides* ($n = 6$). *$P = 0.0339$, 95% CI: −1,737, −84.64; **$P = 0.0083$, 95% CI: 1,365, 6,150. **k**, Quantify of *B. vulgatus* in mouse faeces ($n = 6$). ****$P < 0.0001$, 95% CI: −0.7138, −0.3373; ****$P < 0.0001$, 95% CI: 4.782, 6.850. **l**, Quantify of *B. vulgatus* in mouse faeces after co-housing ($n = 6$). ****$P < 0.0001$, 95% CI: 2.037, 3.277; ***$P = 0.0001$, 95% CI: −0.5855, −0.2692. **m**, Two-bottle preference assay with sucrose (100 mM) in Gko mice after back-supplementation with *B. vulgatus* ($n = 9$). ****$P < 0.0001$, 95% CI: −0.1942, −0.09768. **n**, Fasting blood glucose levels in Gko mice after back-supplementation with *B. vulgatus* ($n = 9$). *$P < 0.05$, 95% CI: −0.8324, −0.01204. *P* values were determined using unpaired, two-tailed *t*-test. Data represent mean ± s.e.m. For data shown as 'box and whisker' plots: the box extends from the 25th to the 75th percentiles, the centre is the median, and whiskers indicate the minimum and maximum, with all data points shown.

https://doi.org/10.1038/s41564-024-01902-8

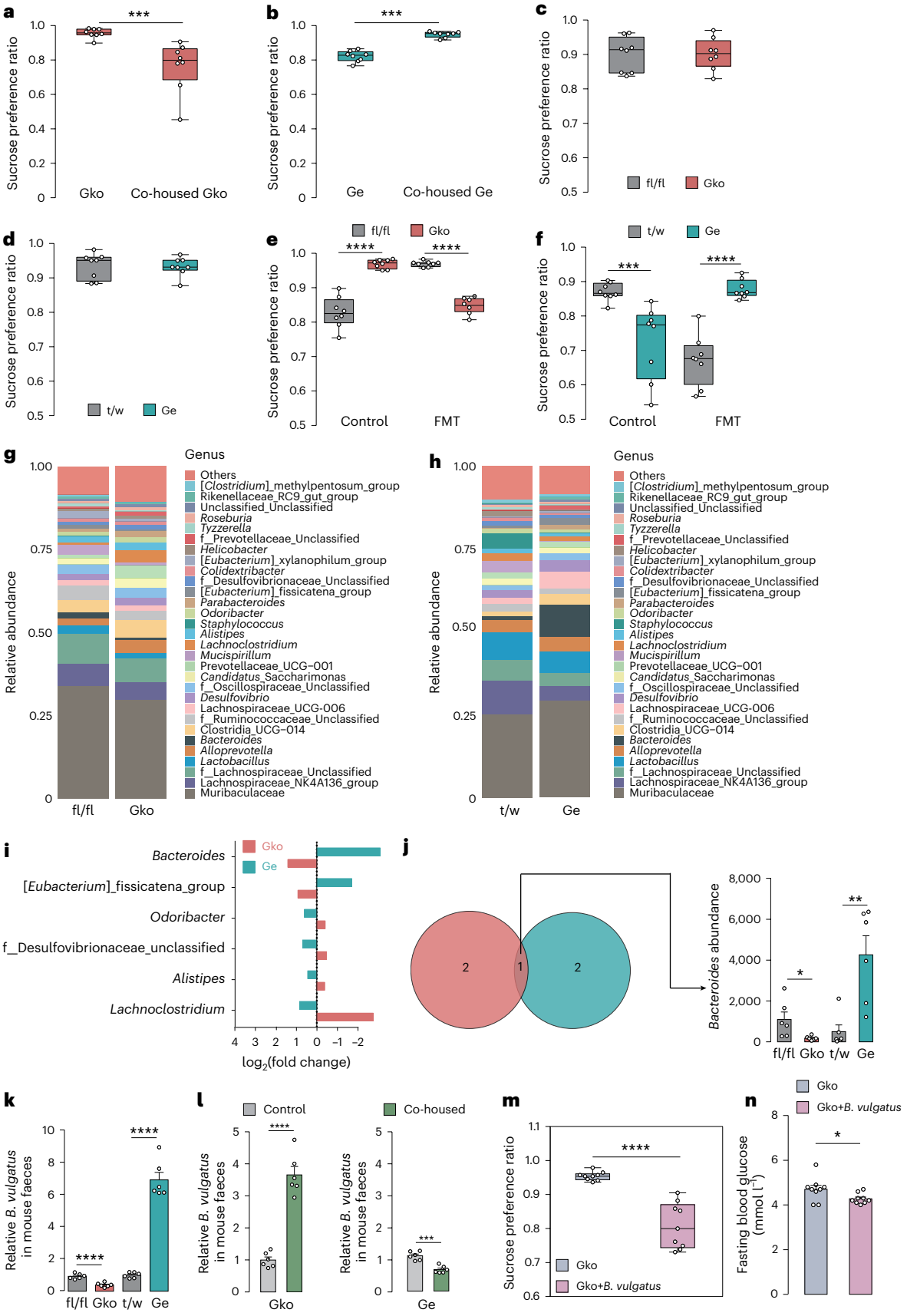

https://doi.org/10.1038/s41564-024-01902-8

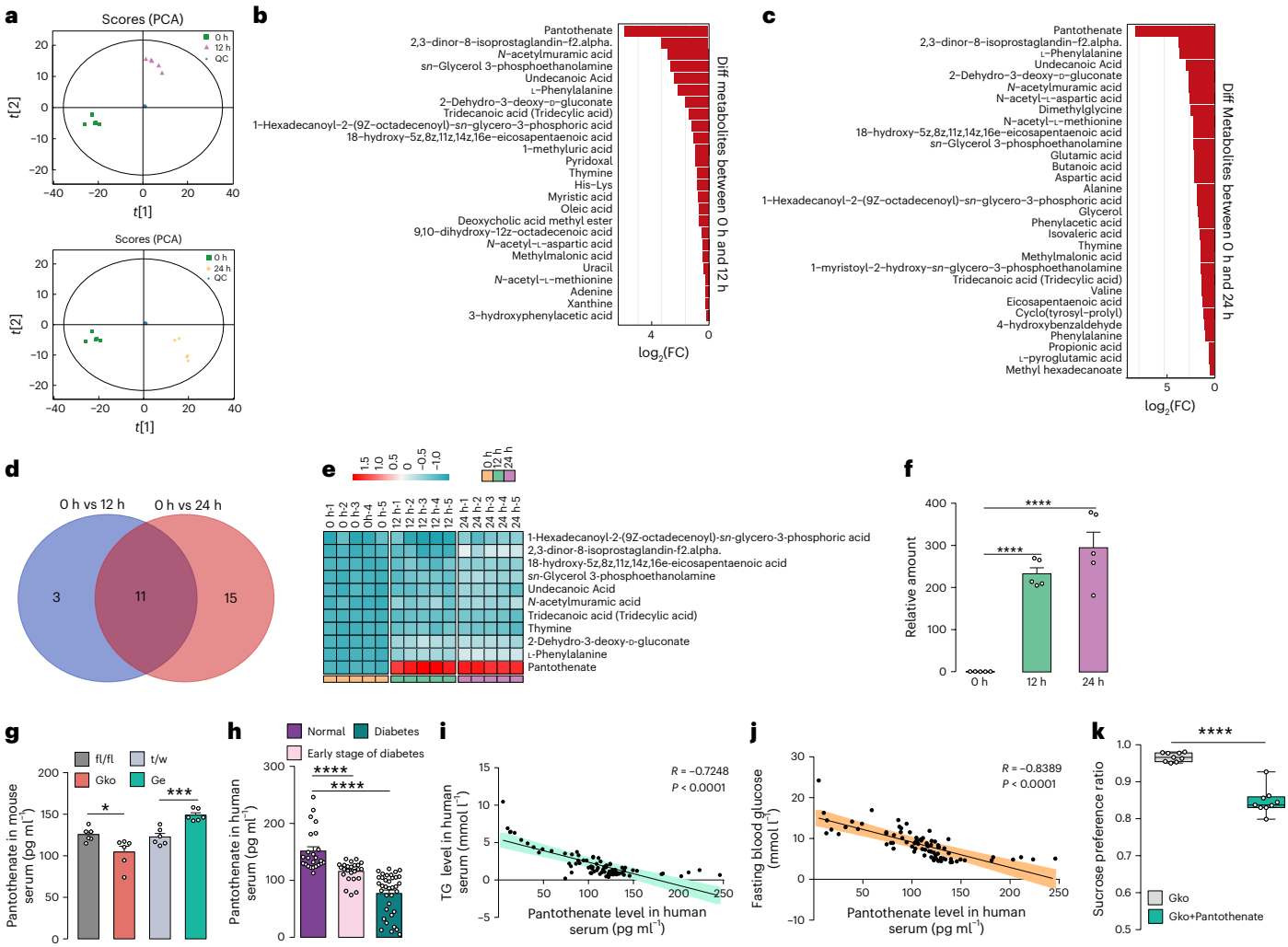

Fig. 5 | Discovery of pantothenate as the key metabolite of *B. vulgatus* via untargeted and targeted metabolomics. a, PCA of metabolites at 0 h vs 12 h and 0 h vs 24 h. **b**, Significantly different metabolite expression at 0 h vs 12 h according to difference ploidy analysis. **c**, Significantly different metabolite expression at 0 h vs 24 h according to difference ploidy analysis. **d**, Wayne plot of significantly different metabolites at 0 h vs 12 h and at 0 h vs 24 h. **e**, Heat map of the relative abundance of overlapping metabolites at 0 h vs 12 h and at 0 h vs 24 h. Colour bar indicates metabolites abundances were $\log_{10}$ transformed. **f**, Relative abundance of pantothenate at 0 h, 12 h and 24 h ($n = 5$). $^{****}P < 0.0001$, 95% CI: 197.6, 263.0; $^{****}P < 0.0001$, 95% CI: 206.8, 376.5. **g**, Pantothenate levels in mouse serum ($n = 6$). $^{*}P = 0.0220$, 95% CI: −38.25, −3.715; $^{***}P = 0.0004$, 95% CI: 14.94, 37.23. **h**, Pantothenate levels in patient serum (normal and early stage of diabetes, $n = 24$; diabetes, $n = 36$). $^{****}P < 0.0001$. **i**, Correlation between pantothenate levels in patient serum and TG levels in patient serum ($n = 24/36$). Shaded area represents 95% confidence intervals. **j**, Correlation between pantothenate levels in patient serum and FBG levels ($n = 24/36$). Shaded area represents 95% confidence intervals. **k**, Two-bottle preference assay with sucrose (100 mM) in Gko mice after supplementation with pantothenate ($n = 9$). $^{****}P < 0.0001$, 95% CI: −0.1461, −0.09384. *P* values were determined using unpaired, two-tailed *t*-test. Data represent mean ± s.e.m. For data shown as 'box and whisker' plots: the box extends from the 25th to the 75th percentiles, the centre is the median, and whiskers indicate the minimum and maximum, with all data points shown.

mice (Extended Data Fig. 6i). Therefore, pantothenate and *B. vulgatus* may be more suitable for improving hyperglycaemia caused by *Ffar4* mutations or inactivation.

To further demonstrate whether pantothenate directly affects GLP-1 secretion, pantothenate was added to the culture medium of STC-1 cells. It was found that pantothenate significantly increased the release of GLP-1 (Fig. 6d), which was consistent with the in vivo experiments. We silenced *Ffar4* in STC-1 cells and then assayed the amount of GLP-1 released after stimulating the cells with pantothenate. Results showed that knockdown of *Ffar4* in STC-1 cells did not affect GLP-1 secretion, but pantothenate promoted GLP-1 secretion in the *Ffar4*-silenced state (Extended Data Fig. 6j,k).

This study also further reveals that epithelial cell-derived Ffar4 itself does not directly affect GLP-1 release from enteroendocrine cells and that it is required to drive the release of GLP-1 through intestinal microbes and their key products as a mediator. To further determine whether GLP-1 administration could inhibit sugar preference in Gko mice, we injected Gko mice with liraglutide[24]. Results showed that sugar preference was significantly reduced in Gko mice treated with liraglutide, a glucagon-like peptide 1 receptor agonist (Fig. 6e). At the same time, we examined the FBG of the mice and found that it was significantly reduced in Gko mice by liraglutide treatment (Extended Data Fig. 6l).

Several studies have shown that GLP-1RAs positively regulate hepatic FGF21 production in rodent models[25,26]. Furthermore, studies have demonstrated that FGF21 is a key regulator of Ffar4, affecting multiple physiological states[27,28], therefore, we hypothesized that FGF21 may act as a direct downstream regulator of GLP-1 in mediating sugar preference. To investigate whether certain sugar preference modulations of liraglutide in mice with dietary challenge rely on the presence of hepatic FGF21, serum FGF21 expression was measured. Serum FGF21 was found to be decreased in Gko mice, while after liraglutide injection,

https://doi.org/10.1038/s41564-024-01902-8

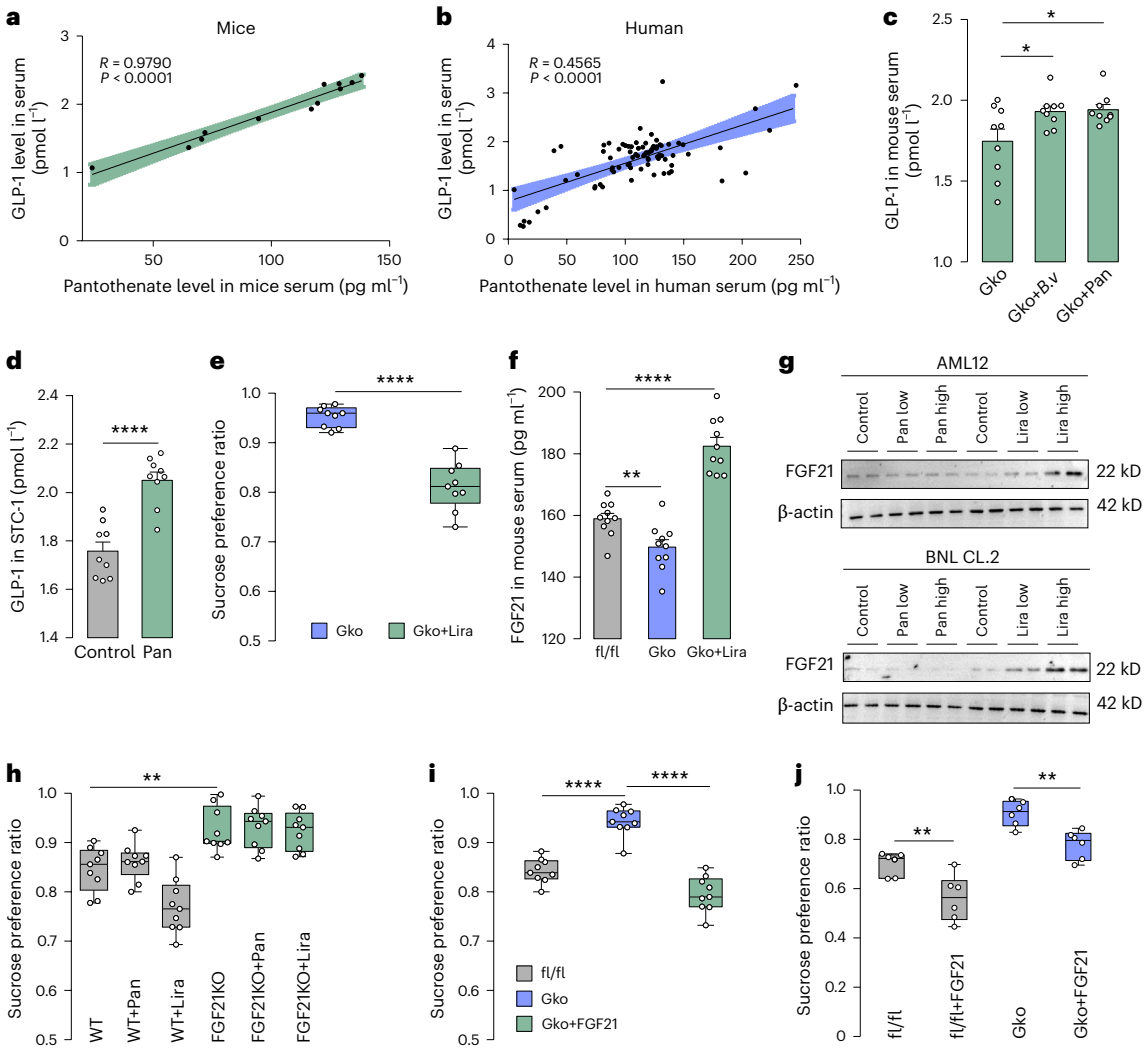

Fig. 6 | Pantothenate alters sugar preference in mice by affecting the GLP-1-FGF21 pathway. a, Correlation between pantothenate levels and GLP-1 levels in mouse serum ($n = 6$). Shaded area represents 95% confidence intervals. **b**, Correlation between pantothenate levels and GLP-1 levels in patient serum ($n = 24/36$). Shaded area represents 95% confidence intervals. **c**, Assay of GLP-1 content in mouse serum ($n = 9$). *$P = 0.0397$, 95% CI: 0.009846, 0.3581; *$P = 0.0292$, 95% CI: 0.02242, 0.3678. **d**, Assay of GLP-1 content in STC-1 cells after pantothenate treatment ($n = 9$). ****$P < 0.0001$, 95% CI: 0.1856, 0.3999. **e**, Two-bottle preference assay with sucrose (100 mM) in Gko mice after supplementation with liraglutide ($n = 9$). ****$P < 0.0001$, 95% CI: −0.1784, −0.1043. **f**, Assay of FGF21 content in mouse serum ($n = 10$). **$P = 0.0067$, 95% CI: −15.47, −2.883; ****$P < 0.0001$, 95% CI: 16.5, 30.57. **g**, Immunoblotting analysis of FGF21 levels in AML12 and BNL CL.2 cells after treatment with pantothenate/liraglutide ($n = 6$). **h**, Two-bottle preference assay with sucrose (100 mM) in WT/FGF21KO mice after supplementation with pantothenate/liraglutide ($n = 9$). **$P = 0.0016$, 95% CI: 0.03498, 0.1244. **i**, Two-bottle preference assay with sucrose (100 mM) in fl/fl and Gko mice after injection with FGF21 ($n = 9$). ****$P < 0.0001$, 95% CI: 0.07275, 0.1267; ****$P < 0.0001$, 95% CI: −0.1801, −0.1144. **j**, Two-bottle preference assay with sucrose (100 mM) in fl/fl and Gko mice after stereotaxic injection with FGF21 ($n = 6$). **$P = 0.0084$, 95% CI: −0.2306, −0.04376; **$P = 0.0026$, 95% CI: −0.1949, −0.05489. *P* values were determined using unpaired, two-tailed *t*-test. Data represent mean ± s.e.m. For data shown as 'box and whisker' plots: the box extends from the 25th to the 75th percentiles, the centre is the median, and whiskers indicate the minimum and maximum, with all data points shown.

FGF21 in Gko serum was significantly upregulated (Fig. 6f). In addition, the serum levels of FGF21 in diabetic mice were significantly lower than those in the control group (Extended Data Fig. 6m).

Furthermore, hepatic FGF21 mRNA and FGF21 protein levels were significantly increased by liraglutide treatment in two normal classic hepatic cells, while pantothenate did not affect FGF21 expression in the two in vitro hepatic cells (Fig. 6g and Extended Data Fig. 6n,o). To further determine whether Ffar4-pantothenate-GLP-1 signalling inhibited sugar preference dependent on FGF21 release, FGF21 recombinant protein[29] and FGF21KO mice were used (Extended Data Fig. 6p). Results showed that FGF21KO mice exhibited increased sugar preference compared with WT mice and FGF21 deletion blocked the sugar preference inhibition of liraglutide or *B. vulgatus* or pantothenate (Fig. 6h and Extended Data Fig. 7a), while FGF21 recombinant protein reversed *Ffar4* deletion-induced sugar preference and elevated fasting glucose (Fig. 6i and Extended Data Fig. 7b).

The ventromedial hypothalamus (VMH) is an important target site for FGF21-mediated sugar intake[15,29,30]. To further confirm the specific site of FGF21 action, we injected FGF21 recombinant protein to the VMH of Gko and fl/fl mice to detect whether it could reverse the sugar preference in Gko mice. We found that the FGF21 recombinant protein inhibited sugar preference in both Gko and fl/fl mice (Fig. 6j). As pantothenate could cross the blood-brain barrier[31], we further injected pantothenate into the VMH of Gko mice and measured sugar preferences. Results showed that pantothenate did not alter the sugar preference of Gko mice (Extended Data Fig. 7c). We further silenced the GLP-1R (AAV9-shGlp1r-u6-EGFP) of the VMH region in Gko mice to assess whether VMH region GLP-1R signalling influenced sugar preference.

Results showed that the expression level of GLP-1R in the brain area was significantly reduced after virus injection (Extended Data Fig. 7d,e), and the knockdown GLP-1R did not affect the reduction of sugar preference in Gko mice gavaged with *B. vulgatus* and pantothenate (Extended Data Fig. 7f). In conclusion, Ffar4 regulated the abundance of *B. vulgatus*, whose derived key metabolite pantothenate further activated the GLP-1-FGF21 axis, thereby shaping the sugar preference homeostasis (Extended Data Fig. 8).

Discussion

A growing body of research has revealed that our cravings for dietary components originate from signals sent from the gut, a key organ in transmitting dietary preferences[32]. However, which genes, gut flora and metabolites in the gut microenvironment are involved in the regulation of sugar preference is currently unclear.

Ffar4 is the major receptor of human dietary fatty acids and most studies have focused on its role in fatty acid signal transduction and lipid metabolism[33]. However, large-scale clinical studies have suggested that only hyperglycaemia occurs in the *Ffar4*-mutated population[18]. In the present study, we identified a potential role for Ffar4 in dietary preference. Intestinal Ffar4 deficiency significantly reduces the abundance of the intestinal bacterial colony *B. vulgatus*, and pantothenic acid—a key metabolite of *B. vulgatus*—can directly affect intestinal GLP-1 secretion and further promote hepatic FGF21 release, which then modulates ingestive sugar preference. Our findings shed new light on why people with *Ffar4* mutations develop elevated FBG, and Ffar4 activation or supplementation with probiotics that produce high levels of pantothenic acid may be a strategy to prevent diabetes.

Several studies have shown that probiotic supplementation is an excellent way to regulate the gut to prevent metabolic diseases[34–39]. *Lactobacillus plantarum* reduces FBG in T2D rats[40]; butyrate metabolized by intestinal microorganisms improves insulin sensitivity[41]; and *Bacteroides uniformis* reduces hepatic triglyceride levels and improves metabolic dysfunction[42,43]. In this paper, we provide a genetic approach to screen potential probiotics by manipulating the expression of key genes, and we have screened pantothenic acid-rich *B. vulgatus* in this way. A previous study found that *B. vulgatus* was a key species driving the association between biosynthesis of branched-chain amino acids and insulin resistance by integrating human gut microbiome data[34]. Despite this, the role of *B. vulgatus* in insulin resistance and metabolic disorders seems complex, and omics analytes do not reflect a real effect of the *B. vulgatus* in vivo. Several studies have found that *B. vulgatus* inhibits the development of metabolic disorders in low-fat diet[44] and regulated the TGR5 signalling pathway to improve glucolipid metabolism[45]. Meanwhile, our results indicated that Ffar4 regulated the abundance of *B. vulgatus*, whose derived key metabolite pantothenate further activated the GLP-1-FGF21 axis, thereby shaping the sugar preference homeostasis.

This study sheds light on how Ffar4 expressed in intestinal epithelial cells regulates gut hormone secretion in enteroendocrine cells by impacting the gut microbiota. GLP-1 is a multifaceted hormone with broad pharmacological potential. Studies have shown that GLP-1 can stimulate the secretion of FGF21 in the liver[25,46], which is consistent with our results. FGF21 is a liver-derived hormone that signals to the brain to regulate macronutrient intake and energy homeostasis[47]. Research has shown that FGF21 administration signals to glutamatergic neurons in the VMH to suppress sugar intake[48]. Our results indicate that pantothenate boosted the release of GLP-1, which in turn stimulated hepatic FGF21 expression and regulated the sugar intake in mice. Several studies have shown that VMH is a key region in glucose sensing and the regulation of glucose homeostasis[49,50], while FGF21 acts directly in the VMH to specifically regulate sugar intake[29]. Therefore, we focused on the role of gut–liver axis stimulated hepatic FGF21 on the sugar preference in the VMH and assessed whether GLP-1R signalling in the VMH region influenced sugar preference. We observed that the knockdown GLP-1R did not affect the reduction of sugar preference in Gko mice gavaged with *B. vulgatus* and pantothenate. These results further confirmed that FGF21 was a direct effector protein that regulated sugar preference. Sugar preference is also associated with the endocannabinoid and mesolimbic dopaminergic systems, which are involved in brain reward systems and the regulation of motivational processes. Thus, future research needs to explore whether the brain reward system is involved in the Ffar4-mediated sugar preference.

In conclusion, our study suggests that intestinal Ffar4 deficiency leads to increased sugar preference in mice, which may be an important contributor to the development of diabetes. We demonstrated a mechanism affecting sugar preference in mice through gut–liver–brain interactions via which *B. vulgatus*-derived pantothenate mediated the GLP-1-FGF21 hormone axis. Our study also provides a strategy for diabetes prevention, and the development of Ffar4 tissue-specific agonists may be another approach for diabetes prevention.

Methods

Human participants

We obtained peripheral blood samples from a total of 60 individuals with type 2 diabetes and from 24 healthy controls. All participants with type 2 diabetes met the diagnostic criteria established by the American Diabetes Association. The *Ffar4* mRNA expression of peripheral blood was assessed using RT–qPCR. The Medical Ethics Committee of Jiangnan University (Ref. No. JNU20210310IRB01) approved the collection of peripheral blood from both patients with diabetes and healthy donors. We also collected faecal samples from 45 patients with type 2 diabetes and 15 healthy controls. All participants with type 2 diabetes met the diagnostic criteria established by the American Diabetes Association, and all participants had not received any antibiotics or laxatives during the sample collection. We quantified the *B. vulgatus* content in faeces, and the data were homogenized (Medical Ethics Review Approval Document of Wuxi Second People's Hospital: 2024-Y-156). Before their inclusion in the study, all participants or their legal guardians provided written informed consent.

Animals

The mice in the mouse experiment were all male. All *Ffar4*-knockout (KO, RRID: MGI: 7256540) mice, Villin-Cre mice and Alb-Cre mice were obtained from Shanghai Bioraylab and Shanghai Biomodel Organism. Floxed *Ffar4* (fl/fl, RRID: MGI: 7256541) and *Ffar4* transgenic (t/w, RRID: MGI: 7256542) mice were constructed commercially by the Shanghai Biomodel Organism and the Nanjing Biomedical Research Institute of Nanjing University, respectively. All *FGF21*-knockout (strain no. T012638), db/db and db/m mice were purchased from GemPharmatech. All mice were housed in enriched environments under specific pathogen-free (SPF) conditions. Corncob bedding was provided and the mice had ad libitum access to autoclaved food and water. The housing facility was maintained at a temperature range of 19–26 °C and a humidity level of 40–70%. The mice were housed under a 12-h light/dark cycle. All animal procedures adhered to the Guide for the Care and Use of Laboratory Animals of the School of Medicine, Jiangnan University, and were approved by the Animal Ethics Committee of Jiangnan University (JN No. 20200515t0030810).

Surgery

Mice (8-week-old) were anaesthetized with 2–3% isofluorane and placed on a stereotaxic frame. Heat pads were used through the duration of the surgery to keep the body temperature stable. Eye ointment was applied to keep the eyes from drying. An incision was made to the skin to expose the skull after asepsis with Betadine and medical alcohol was applied. Drug infusions were administered using an internal cannula on the VMH (AP −1.46; ML ±0.6; DV −5.3) of mice at a rate of 0.2 μl min^{-1}. For GLP-1R silencing, AAV9-shGlp1r-u6-EGFP (Shanghai Genechem) or control AAV were injected into the VMH (AP −1.46; ML ±0.6; DV −5.3) of

cKO mice, with a 1 µl injection of 1×10^{12} vg ml^{-1} (virus genome/ml) at a rate of 0.2 µl min^{-1}. The syringe was left in place for 5 min after completion of the injection.

Microglia isolation

Microglia were isolated as previously described[51,52]. Briefly, mice were anaesthetized with isoflurane and perfused with ice-cold saline. Brain tissues were freshly collected in Hanks' balanced salt solution (HBSS) buffer and then digested in HBSS containing collagenase type 2 (37.5 U ml^{-1}) and DNase I (45 U ml^{-1}) for 30 min at 37 °C. Brain tissue homogenates were filtered with a 70-mm cell strainer and then centrifuged at 600 *g* for 5 min (4 °C) to collect the cell pellets. Microglia were isolated by density gradient centrifugation. Collected cell pellets were then suspended in 37% Percoll solution, added into 15-ml centrifuge tubes (SAINING, 3031100) with 70% Percoll, 37% Percoll and PBS (NEST Biotechnology, 211031), and centrifuged at 800 *g* for 30 min (4 °C). Microglia were collected at the interface of the bottom two layers (70%/37%). Microglia were further purified by incubating with CD11b MicroBeads (Precision Biomedicals, 721105) according to manufacturer protocol.

Mouse dietary selection experiment

To investigate dietary preferences in mice, we conducted an experiment using *Ffar4*KO mice. These mice were divided into two groups, with one group being given a 60% high-fat diet (HFD) and a normal diet (ND), and the other group given a 60% high-sugar diet (HSD) and a normal diet (ND). Control WT mice were also included in the experiment. The mice were provided with ad libitum access to food, and the positions of the two diets were changed each day to eliminate any potential effects of position. The amount of food that was consumed by the mice was measured every 24 h, and statistical analysis was performed to compare the daily intake of each diet.

Two-bottle preference assays

To assess the preference of mice for different types of liquid, we conducted two-bottle preference assays using standard mouse cages. The mice were not deprived of water before the experiment and had continuous access to food throughout the experiment. Before the experiment, the mice were allowed to acclimate to cages with two water bottles for 5 days. Subsequently, the mice were given two bottles, one containing only water and the other containing water with various sugar solutions (100 mM sucrose, 100 mM fructose, 100 mM glucose, 2% dextrin, 0.2% saccharin, 0.2% aspartame and 1.5 mM quinine). The daily consumption of both types of water was measured for 5 consecutive days, and the positions of the water bottles were changed each day to avoid any biases caused by the effects of position.

Mice co-housing experiment

To examine the effects of co-housing on mice, we conducted an 8-week experiment using various mouse strains. *Ffar4*KO mice and WT mice were divided into equal proportions and housed together in cages, with each cage containing 4 *Ffar4*KO mice and 4 WT mice. This setup was replicated in a total of 3 cages. Similarly, Gko mice and fl/fl mice, as well as Ge mice and t/w mice, were divided into equal proportions and co-housed in separate cages. The control groups consisted of 3 cages containing either 4 *Ffar4*KO mice or 4 WT mice, 4 Gko mice or 4 fl/fl mice, and 4 Ge mice or 4 t/w mice per cage. This co-housing experiment was conducted for a duration of 8 weeks.

Mouse faecal microbiota transplantation experiment

*Ffar4*KO/Gko/Ge mice (8-week-old) and WT/fl/fl/t/w mice were treated with ABX (1 g l^{-1} metronidazole (Sigma-Aldrich), 0.5 g l^{-1} vancomycin (Sigma-Aldrich), 1 g l^{-1} ampicillin (Sigma-Aldrich) and 1 g l^{-1} neomycin (Sigma-Aldrich))[53] by daily oral gavage of 200 µl for 7 days. We collected fresh faeces (360 mg) from normal *Ffar4*KO/Gko/Ge mice and WT/fl/fl/t/w mice and placed them in 3 ml of transfer buffer (pre-reduced sterile PBS containing 0.05% cysteine HCl on ice). The faeces were homogenized, centrifuged at 800 *g* for 2 min, and faecal supernatant was orally inoculated to mice at 100 µl day^{-1} for 30 days.

16S ribosomal RNA gene sequencing and analysis

DNA was extracted using the HiPure Stool DNA kit. The concentration of DNA was assessed using the Qubit dsDNA HS Assay kit. 16S rRNA gene sequencing was performed by Genewiz. For the filtering process, the double-end sequencing reads were combined; only sequences with lengths greater than 200 bp were retained, and any sequences containing the letter 'N' were removed. Subsequently, the sequences were quality filtered and chimaeric sequences were purified. The resulting sequences were then used for operational taxonomic unit (OTU) clustering via VSEARCH clustering (v.1.9.6) with a sequence similarity threshold of 97% against the Silva 138 16S rRNA reference database. Representative sequences were taxonomically classified using the Ribosomal Database Program (RDP) classifier Bayesian algorithm, and the community composition of each sample was analysed at various levels of species classification. The obtained results were based on an analysis of the OTUs. The method that was used to obtain these results involved random sampling of sample sequences, which ensured a flat distribution. To assess the diversity of the community, various indices, such as Shannon, Chao1 alpha diversity, abundance and evenness of community species, as well as rarefaction curves and rank-abundance graphs, were used. These indicators provide insight into the richness and evenness of species within a community. To determine whether there were significant differences in the microbial communities between samples, (un)weighted UniFrac analysis was conducted and results compared. In addition, beta diversity visualization was performed using principal component analysis (PCA), principal coordinate analysis and non-metric multidimensional scaling. PCA is based on the abundance of OTUs in the sample, while principal coordinate analysis and non-metric multidimensional scaling utilize the distance matrix of the community. To further understand the relationship among samples, a UPGMA clustering tree was constructed using weighted clustering hierarchy and the group average method. Analysis of similarities was used to examine the significance of differences between rank values in the analysis group and rank differences within the group. This analysis provided insight into whether there are notable differences among groups. Metastats gap analysis was performed to rigorously evaluate differences in species abundance between two groups of microbial communities. LEfSE analysis was performed to illustrate the hierarchical evolution of microbial community structure and species differences between groups. This analysis highlights the differences between groups and presents them in a branching tree diagram.

Culture of *B. vulgatus*

B. vulgatus was cultivated in brain–heart infusion medium under strict anaerobic conditions. The medium was supplemented with 50 ng l^{-1} L-cysteine to support growth. The colony-forming units per millilitre (c.f.u.s ml^{-1}) were determined using anaerobic plate counting on brain–heart infusion agar medium (2% agar) with a representative culture stock. For bacterial preservation, a liquid preparation was prepared by mixing 1‰ cysteine with 60% glycerol in water. The *B. vulgatus* culture was resuspended in 1 ml of medium and mixed with an equal volume of the bacteria-preserving medium, resulting in a final concentration of 2.5×10^9 c.f.u.s ml^{-1}.

Metabolomic analysis

B. vulgatus strains were deposited in Jiangnan University's Culture Collection of Food Microorganisms (CCFM) in Wuxi, China. The strains were grown anaerobically at 37 °C for 18 h in brain–heart infusion broth (Hopebio) supplemented with 5 µg ml^{-1} hemin (Sangon Biotech) and

0.5 μg ml^{-1} vitamin K1 (Sangon Biotech). To obtain a fresh culture of each strain, centrifugation was performed for 5 min at 6,000 *g*, followed by two washes with sterile phosphate-buffered saline (PBS). The resulting bacterial pellets were then resuspended in sterile PBS at a concentration of 5×10^9 c.f.u.s ml^{-1}. The suspended mixtures were transferred into new centrifuge tubes and subjected to centrifugation at 14,000 × *g* for 20 min to collect the supernatants. For LC–MS analysis, the samples were redissolved in a solvent consisting of 100 μl acetonitrile/water (1:1, v/v), after which they were centrifuged at 14,000 *g* at 4 °C for 15 min. The resulting supernatants were then injected into the system. Subsequently, the supernatants were dried using a vacuum centrifuge. Quality control (QC) samples were prepared by pooling 10 μl of each sample, and these samples were analysed alongside the other samples to monitor instrument analysis stability and repeatability. These QC samples were regularly inserted and analysed every 5 samples.

Cell culture

STC-1 cells, AML12 cells and BNL CL.2 cells were obtained from the National Collection of Authenticated Cell Cultures and cultured in DMEM (Gibco, C11965500) or DMEM/F12 medium (BasalMedia Technologies, L310KJ) supplemented with 5% fetal bovine serum (FBS, VivaCell Biotechnology, C04001) and 1% penicillin–streptomycin at 37 °C and 5% CO_2.

Small interfering RNA (siRNA) transfection

STC-1 cells were cultured until they reached 50–70% confluence, after which they were transfected with *Ffar4*-targeting siRNA (50 pM) or NC siRNA (50 pM) using jetPRIME transfection reagent (Polyplus, 114-15) following manufacturer protocol. The siRNA sequence for mouse *Ffar4* was as follows: ACCGCAUAGGAGAAAUCUCAUTT. A universal negative control siRNA (GenePharma, A06001) was used as a reference. Following a 24-h stimulation with pantothenate, the secretion of GLP-1 was analysed.

Treatment of mice with pantothenate/liraglutide/FGF21

Gko/WT mice (8-week-old) were treated with pantothenate (10 mg kg^{-1} day^{-1})[54] for 10 days, while the control group was treated with saline. Fasting blood glucose tests were conducted, and samples were collected following euthanasia after the completion of the double water bottle choice test. Gko/FGF21KO/WT mice (8-week-old) were treated with liraglutide (200 μg kg^{-1} day^{-1}) for 5 days[55], while the control group was treated with saline. Fasting blood glucose tests were conducted, and samples were collected following euthanasia after the completion of the double water bottle choice test. Gko/WT mice (8-week-old) were treated with FGF21 (1 mg kg^{-1} day^{-1}) for 7 days[29], while the control group was treated with saline. Fasting blood glucose tests were conducted, and samples were collected following euthanasia after the completion of the double water bottle choice test.

Recombinant protein

Recombinant FGF21 protein was expressed and purified as previously described[56,57].

Quantitative real-time polymerase chain reaction (qPCR)

Total RNA was extracted using a FastPure Cell/Tissue Total RNA Isolation Kit V2 (Vazyme, RC112-01) according to manufacturer instructions. The RNA was then reverse transcribed into complementary DNA using the HiScript III 1st Strand cDNA synthesis kit (Vazyme, R323-01). RT–qPCR was performed using the Roche LightCycler 480 PCR System and the Hieff UNICON qPCR SYBR Green Master Mix (Shanghai YEASEN Biotech, 11198ES). Expression of the target genes was evaluated using the $2^{-\Delta\Delta Ct}$ method and normalized to β-actin gene expression. The RT–qPCR primer sequences can be found in Supplementary Table 1.

Western blotting

To analyse the total protein content of AML12 and BNL CL.2 cells, we utilized RIPA buffer to lyse the cells. Western blotting was performed as previously described[58]. The protein samples were separated with 10–12% SDS–PAGE gels and subsequently transferred to polyvinylidene difluoride (PVDF) membranes with a pore size of 0.45 mm. Then, the membranes were blocked for 60 min using 5% non-fat milk and washed three times with Tris buffered saline with Tween 20 (TBST). Primary antibodies against FGF21 (ABclonal, A3908) and β-actin (ABclonal, AC026) were then applied to the PVDF membranes and incubated overnight at 4 °C. Next, the membranes were washed with TBST and incubated with secondary antibodies at room temperature for 2 h. The secondary antibody was HRP-conjugated goat anti-mouse IgG H&L (Biodragon, BF03009). Membrane visualization was achieved by employing an enhanced chemiluminescent (ECL) reagent (Millipore, WBKLS0500).

Enzyme-linked immunosorbent assay

Blood samples were collected via retro-orbital bleeding and portal vein bleeding of male mice, and fresh blood was collected in separate gel coagulation tubes (Kangweishi Medical, 03). Serum was collected after centrifugation (2,500 × *g*, 10 min at 4 °C). Measurement of GLP-1/CCK/PPY/GIP/pantothenate/FGF21 levels in mouse serum or patient serum was performed using specific ELISA kits. We used a mouse GLP-1 ELISA kit (Shanghai Enzyme-linked Biotechnology, ml201801) to measure the GLP-1 levels, a mouse CCK ELISA kit (Shanghai Enzyme-linked Biotechnology, ml058435) to measure the CCK levels, a mouse PYY ELISA kit (Shanghai Enzyme-linked Biotechnology, ml037648) to measure the PYY levels, a mouse GIP ELISA kit (Shanghai Enzyme-linked Biotechnology, ml057748) to measure the GIP levels, a pantothenate ELISA kit (Shanghai Enzyme-linked Biotechnology, ml021743) to measure the pantothenate levels and a mouse FGF21 ELISA kit (Shanghai Enzyme-linked Biotechnology, ml202310) to measure the FGF21 levels. In addition, we used the human GLP-1 ELISA kit (Shanghai Enzyme-linked Biotechnology, ml037425) following manufacturer instructions.

Statistical analysis

No animals or data points were excluded from the analyses. All data were analysed using GraphPad Prism 9.0. Data are presented as mean ± s.e.m. The distribution of the data was tested for normality using the Kolmogorov–Smirnov test. We used Student's *t*-test or one-way analysis of variance (ANOVA) with Tukey's post hoc test for normally distributed variables and Mann–Whitney *U*-test or Kruskal-Wallis with Dunn's post hoc test for non-normally distributed data. Correlation was investigated using Spearman's test with Bonferroni correction. $P < 0.05$ was considered significant.

Reporting summary

Further information on research design is available in the Nature Portfolio Reporting Summary linked to this article.

Data availability

All 16S rRNA gene amplicon sequencing data were deposited at the NCBI under the accession code PRJNA1186342. The metabolomics data were deposited in the MetaboLights MTBLS11684. All data are available in the main text, extended data or supplementary materials. Source data are provided with this paper.

Code availability

No custom code was developed for the analysis of data presented in this paper.

References

1. Eckel, R. H., Bornfeldt, K. E. & Goldberg, I. J. Cardiovascular disease in diabetes, beyond glucose. *Cell Metab.* **33**, 1519–1545 (2021).

2. Ma, X. et al. Excessive intake of sugar: an accomplice of inflammation. *Front. Immunol.* **13**, 988481 (2022).
3. Huang, Y. et al. Dietary sugar consumption and health: umbrella review. *BMJ* **381**, e071609 (2023).
4. Imamura, F. et al. Consumption of sugar sweetened beverages, artificially sweetened beverages, and fruit juice and incidence of type 2 diabetes: systematic review, meta-analysis, and estimation of population attributable fraction. *BMJ* **351**, h3576 (2015).
5. Daher, M. I., Matta, J. M. & Abdel Nour, A. M. Non-nutritive sweeteners and type 2 diabetes: should we ring the bell? *Diabetes Res. Clin. Pract.* **155**, 107786 (2019).
6. Liu, W. W. & Bohórquez, D. V. The neural basis of sugar preference. *Nat. Rev. Neurosci.* **23**, 584–595 (2022).
7. Yan, Y. et al. Reconsolidation of a post-ingestive nutrient memory requires mTOR in the central amygdala. *Mol. Psychiatry* **26**, 2820–2836 (2021).
8. Nikolova, V. L. et al. Perturbations in gut microbiota composition in psychiatric disorders: a review and meta-analysis. *JAMA Psychiatry* **78**, 1343–1354 (2021).
9. Komaroff, A. L. The microbiome and risk for obesity and diabetes. *JAMA* **317**, 355–356 (2017).
10. de Wouters d'Oplinter, A. et al. Gut microbes participate in food preference alterations during obesity. *Gut Microbes* **13**, 1959242 (2021).
11. Swartz, T. D., Duca, F. A., de Wouters, T., Sakar, Y. & Covasa, M. Up-regulation of intestinal type 1 taste receptor 3 and sodium glucose luminal transporter-1 expression and increased sucrose intake in mice lacking gut microbiota. *Br. J. Nutr.* **107**, 621–630 (2012).
12. Bernard, A. et al. A preventive prebiotic supplementation improves the sweet taste perception in diet-induced obese mice. *Nutrients* **11**, 549 (2019).
13. Meyer, K. et al. Association of the gut microbiota with cognitive function in midlife. *JAMA Netw. Open* **5**, e2143941 (2022).
14. van de Wouw, M., Schellekens, H., Dinan, T. G. & Cryan, J. F. Microbiota-gut-brain axis: modulator of host metabolism and appetite. *J. Nutr.* **147**, 727–745 (2017).
15. von Holstein-Rathlou, S. et al. FGF21 mediates endocrine control of simple sugar intake and sweet taste preference by the liver. *Cell Metab.* **23**, 335–343 (2016).
16. Loona, D. P. S., Das, B., Kaur, R., Kumar, R. & Yadav, A. K. Free fatty acid receptors (FFARs): emerging therapeutic targets for the management of diabetes mellitus. *Curr. Med. Chem.* **30**, 3404–3440 (2023).
17. Kimura, I., Ichimura, A., Ohue-Kitano, R. & Igarashi, M. Free fatty acid receptors in health and disease. *Physiol. Rev.* **100**, 171–210 (2020).
18. Bonnefond, A. et al. Contribution of the low-frequency, loss-of-function p.R270H mutation in FFAR4 (GPR120) to increased fasting plasma glucose levels. *J. Med. Genet.* **52**, 595–598 (2015).
19. Wang, W. et al. Microglial Ffar4 deficiency promotes cognitive impairment in the context of metabolic syndrome. *Sci. Adv.* **10**, eadj7813 (2024).
20. Jean, S., Wallace, M. J., Dantas, G. & Burnham, C. D. Time for some group therapy: update on identification, antimicrobial resistance, taxonomy, and clinical significance of the *Bacteroides fragilis* group. *J. Clin. Microbiol.* **60**, e0236120 (2022).
21. Jiang, X., Yang, Q., Qu, H., Chen, Y. & Zhu, S. Endogenous n-3 PUFAs improve non-alcoholic fatty liver disease through FFAR4-mediated gut-liver crosstalk. *Nutrients* **15**, 586 (2023).
22. Sankoda, A. et al. Long-chain free fatty acid receptor GPR120 mediates oil-induced GIP secretion through CCK in male mice. *Endocrinology* **158**, 1172–1180 (2017).
23. Peiris, M. et al. Decoy bypass for appetite suppression in obese adults: role of synergistic nutrient sensing receptors GPR84 and FFAR4 on colonic endocrine cells. *Gut* **71**, 928–937 (2022).
24. Meurot, C. et al. Liraglutide, a glucagon-like peptide 1 receptor agonist, exerts analgesic, anti-inflammatory and anti-degradative actions in osteoarthritis. *Sci. Rep.* **12**, 1567 (2022).
25. Liu, D. et al. Hepatic fibroblast growth factor 21 is involved in mediating functions of liraglutide in mice with dietary challenge. *Hepatology* **74**, 2154–2169 (2021).
26. Newsome, P. N. & Ambery, P. Incretins (GLP-1 receptor agonists and dual/triple agonists) and the liver. *J. Hepatol.* **79**, 1557–1565 (2023).
27. Quesada-López, T. et al. The lipid sensor GPR120 promotes brown fat activation and FGF21 release from adipocytes. *Nat. Commun.* **7**, 13479 (2016).
28. Quesada-López, T. et al. GPR120 controls neonatal brown adipose tissue thermogenic induction. *Am. J. Physiol. Endocrinol. Metab.* **317**, E742–e750 (2019).
29. Jensen-Cody, S. O. et al. FGF21 signals to glutamatergic neurons in the ventromedial hypothalamus to suppress carbohydrate intake. *Cell Metab.* **32**, 273–286.e6 (2020).
30. Hultman, K. et al. The central fibroblast growth factor receptor/beta klotho system: comprehensive mapping in *Mus musculus* and comparisons to nonhuman primate and human samples using an automated in situ hybridization platform. *J. Comp. Neurol.* **527**, 2069–2085 (2019).
31. Uchida, Y. et al. Major involvement of Na^+-dependent multivitamin transporter (SLC5A6/SMVT) in uptake of biotin and pantothenic acid by human brain capillary endothelial cells. *J. Neurochem.* **134**, 97–112 (2015).
32. Li, M. et al. Gut–brain circuits for fat preference. *Nature* **610**, 722–730 (2022).
33. Ichimura, A. et al. Dysfunction of lipid sensor GPR120 leads to obesity in both mouse and human. *Nature* **483**, 350–354 (2012).
34. Pedersen, H. K. et al. Human gut microbes impact host serum metabolome and insulin sensitivity. *Nature* **535**, 376–381 (2016).
35. Zhao, L. et al. Gut bacteria selectively promoted by dietary fibers alleviate type 2 diabetes. *Science* **359**, 1151–1156 (2018).
36. Boulangé, C. L., Neves, A. L., Chilloux, J., Nicholson, J. K. & Dumas, M. E. Impact of the gut microbiota on inflammation, obesity, and metabolic disease. *Genome Med.* **8**, 42 (2016).
37. Chobot, A., Górowska-Kowolik, K., Sokołowska, M. & Jarosz-Chobot, P. Obesity and diabetes—not only a simple link between two epidemics. *Diabetes Metab. Res. Rev.* **34**, e3042 (2018).
38. Peters, B. A. et al. A taxonomic signature of obesity in a large study of American adults. *Sci. Rep.* **8**, 9749 (2018).
39. Cani, P. D. Human gut microbiome: hopes, threats and promises. *Gut* **67**, 1716–1725 (2018).
40. Gao, H. et al. Fermented *Momordica charantia* L. juice modulates hyperglycemia, lipid profile, and gut microbiota in type 2 diabetic rats. *Food Res. Int.* **121**, 367–378 (2019).
41. Vrieze, A. et al. Transfer of intestinal microbiota from lean donors increases insulin sensitivity in individuals with metabolic syndrome. *Gastroenterology* **143**, 913–916.e7 (2012).
42. Powell, M. F. & Bruice, T. C. Hydride vs. electron transfer in the oxidation of NADH model compounds. *Prog. Clin. Biol. Res.* **274**, 369–385 (1988).
43. Moonen, W. A. & Festen, C. The treatment of functional disorders of the bladder in spina bifida aperta. *Arch. Chir. Neerl.* **17**, 119–135 (1965).
44. Ridaura, V. K. et al. Gut microbiota from twins discordant for obesity modulate metabolism in mice. *Science* **341**, 1241214 (2013).

45. Chen, B. et al. Glycoursodeoxycholic acid regulates bile acids level and alters gut microbiota and glycolipid metabolism to attenuate diabetes. *Gut Microbes* **15**, 2192155 (2023).
46. Liu, D. et al. Comparison of beneficial metabolic effects of liraglutide and semaglutide in male C57BL/6J mice. *Can. J. Diabetes* **46**, 216–224.e2 (2022).
47. Le, T. D. V. et al. Fibroblast growth factor-21 is required for weight loss induced by the glucagon-like peptide-1 receptor agonist liraglutide in male mice fed high carbohydrate diets. *Mol. Metab.* **72**, 101718 (2023).
48. Kawasaki, H., Ito, K., Matsushita, T., Takayama, J. & Ohira, M. Primary non-Hodgkin's lymphoma of the skin in children. *Acta Paediatr.* **83**, 1315–1316 (1994).
49. Andermann, M. L. & Lowell, B. B. Toward a wiring diagram understanding of appetite control. *Neuron* **95**, 757–778 (2017).
50. Toda, C. et al. UCP2 regulates mitochondrial fission and ventromedial nucleus control of glucose responsiveness. *Cell* **164**, 872–883 (2016).
51. Sato-Hashimoto, M. et al. Microglial SIRPα regulates the emergence of CD11c^{+} microglia and demyelination damage in white matter. *Elife* **8**, e42025 (2019).
52. Sommer, D. et al. ADAM17-deficiency on microglia but not on macrophages promotes phagocytosis and functional recovery after spinal cord injury. *Brain Behav. Immun.* **80**, 129–145 (2019).
53. Sun, J. et al. Pancreatic β-cells limit autoimmune diabetes via an immunoregulatory antimicrobial peptide expressed under the influence of the gut microbiota. *Immunity* **43**, 304–317 (2015).
54. Zhou, H. et al. Pantothenate protects against obesity via brown adipose tissue activation. *Am. J. Physiol. Endocrinol. Metab.* **323**, E69–E79 (2022).
55. Song, J. X. et al. Liraglutide attenuates hepatic iron levels and ferroptosis in db/db mice. *Bioengineered* **13**, 8334–8348 (2022).
56. Ye, X. et al. Design and pharmaceutical evaluation of bifunctional fusion protein of FGF21 and GLP-1 in the treatment of nonalcoholic steatohepatitis. *Eur. J. Pharm.* **952**, 175811 (2023).
57. Wu, Y. K. et al. Sulforaphane ameliorates non-alcoholic fatty liver disease in mice by promoting FGF21/FGFR1 signaling pathway. *Acta Pharm. Sin.* **43**, 1473–1483 (2022).
58. Jiang, X. et al. Pyruvate dehydrogenase B regulates myogenic differentiation via the FoxP1-Arih2 axis. *J. Cachexia Sarcopenia Muscle* **14**, 606–621 (2023).

Acknowledgements

This work was supported by the National Natural Science Foundation of China (3247090211, S.Z.).

Author contributions

S.Z., Y.Q.C., X.L. and T.Z designed the experiments. T.Z., W.W., J.L., Z.W., S.C., X.Y. and S.S. conducted the experiments. T.Z., W.W. and J.L. analysed the data. T.Z., W.W. and S.Z. wrote the paper. All authors read and approved the final paper.

Competing interests

The authors declare no competing interests.

Additional information

Extended data is available for this paper at https://doi.org/10.1038/s41564-024-01902-8.

Supplementary information The online version contains supplementary material available at https://doi.org/10.1038/s41564-024-01902-8.

Correspondence and requests for materials should be addressed to Xinmiao Liang, Yong Q. Chen or Shenglong Zhu.

Peer review information *Nature Microbiology* thanks Cholsoon Jang, Benjamin Jensen and the other, anonymous, reviewer(s) for their contribution to the peer review of this work.

https://doi.org/10.1038/s41564-024-01902-8

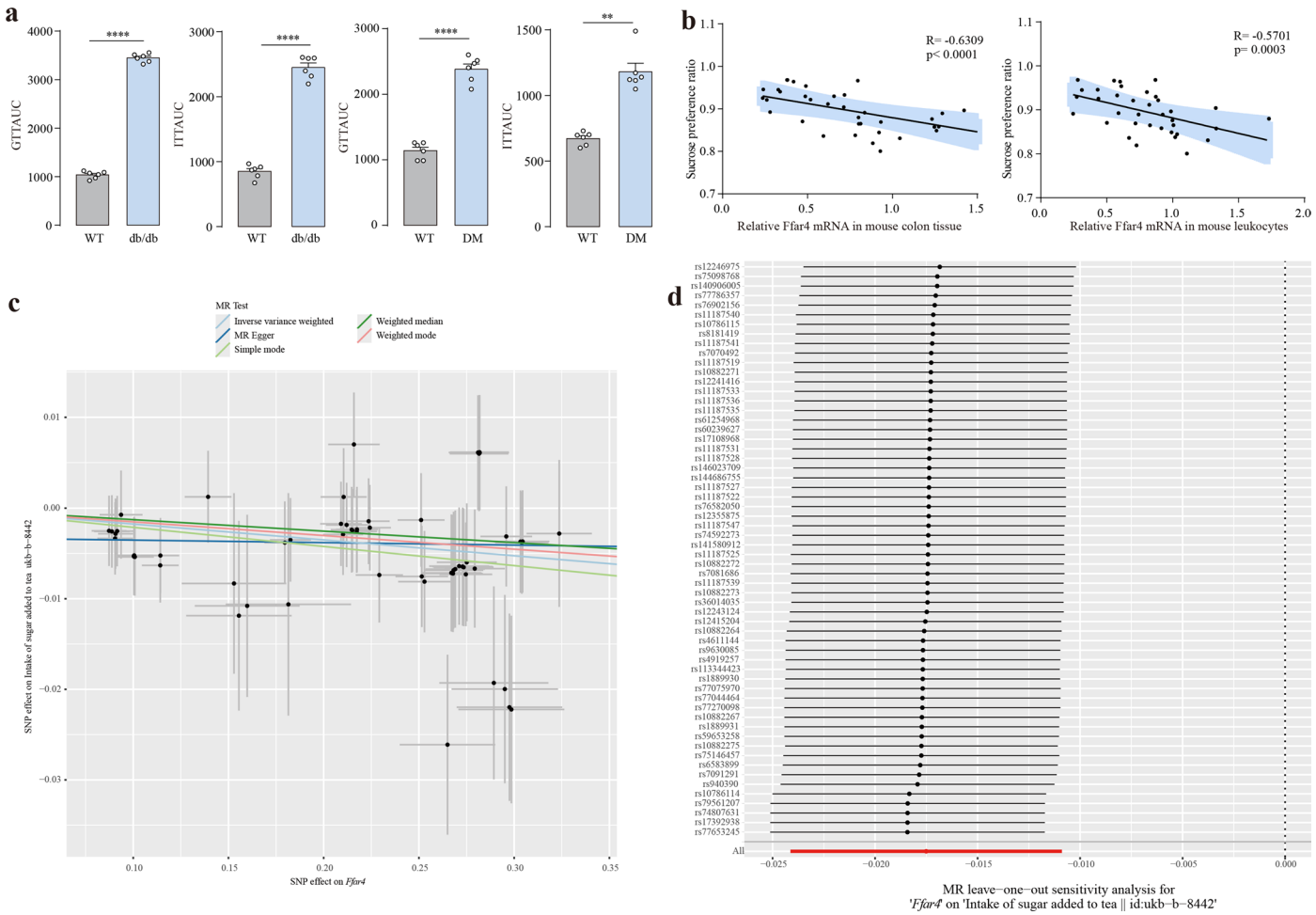

Extended Data Fig. 1 | A Two-sample mendelian randomization. a, The area under the curve (AUC) for both oral glucose tolerance test (GTT) and intraperitoneal glucose tolerance test (ITT) of db/db and DM mouse (n = 6). $p < 0.0001$, 95% Confidence Interval = (2305, 2516); $p < 0.0001$, 95% Confidence Interval = (1415, 1783); $p < 0.0001$, 95% Confidence Interval = (1030, 1453); $p = 0.0022$. **b**, The correlation between Ffar4 levels in mouse colon tissue and mouse sucrose preference (n = 36). The correlation between Ffar4 levels in mouse leukocytes and mouse sucrose preference (n = 36). **c**, Scatter plot of the causal relationship of Ffar4 with sugar added to tea. This plot was used to visualize the effect of each SNP. The horizontal axis represents the exposure effect, and the vertical axis represents the outcome effect. The slopes of the lines represent the causal effect of each method. **d**, Leave-one-out analyses to evaluate whether any single instrumental variable drove the causal effect. p values were determined using unpaired, two-tailed t test. Data represent as mean ± SEM. *p < 0.05, **p < 0.01, *** p < 0.001, ****p < 0.0001.

https://doi.org/10.1038/s41564-024-01902-8

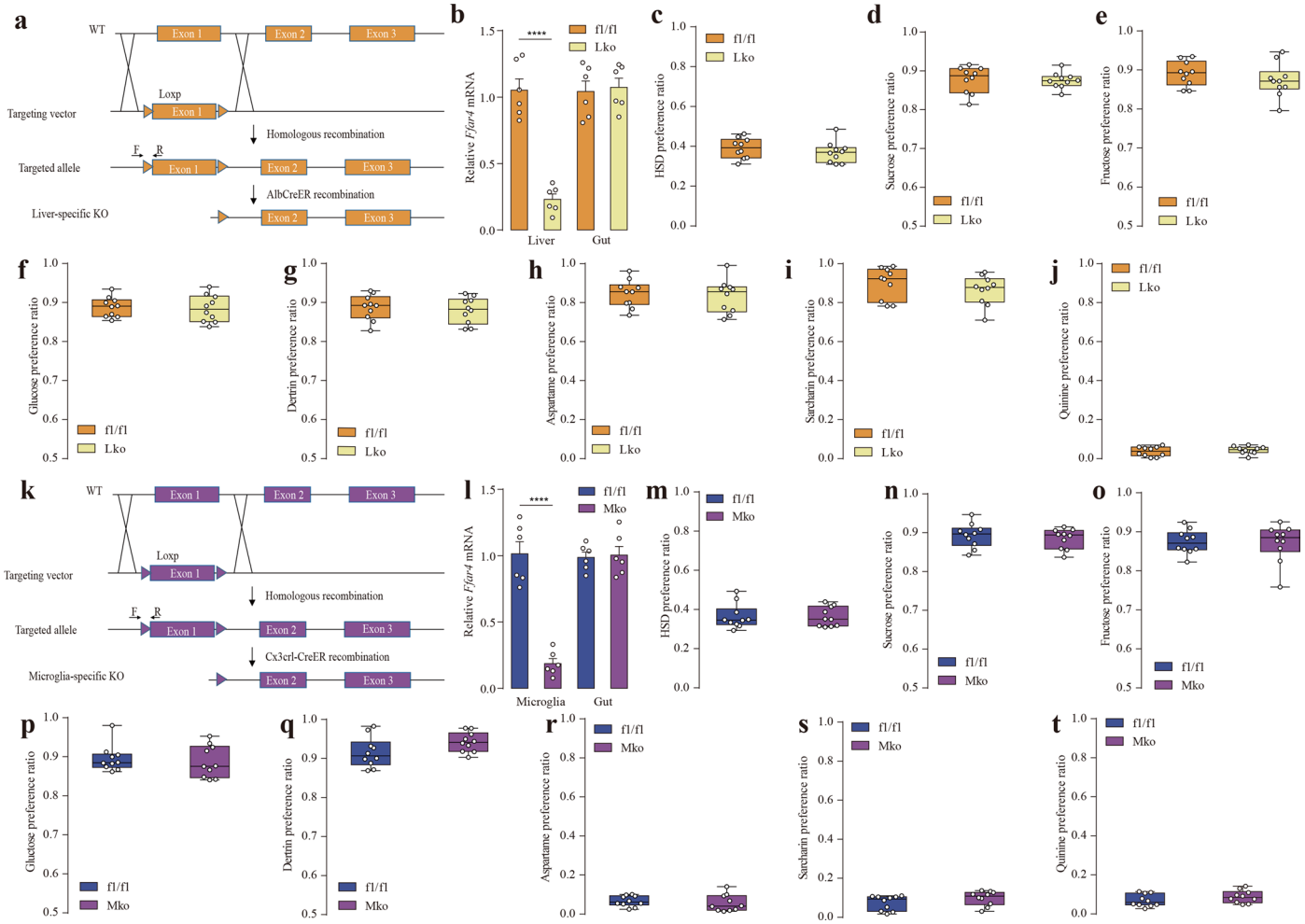

Extended Data Fig. 2 | Effect of liver or microglial Ffar4 deletion on dietary preference in mice. a, We constructed liver-specific knockout mice(Alb-Cre; Ffar4Loxp/Loxp, abbreviated Lko) corresponding control mice (Ffar4Loxp/Loxp) are abbreviated as fl/fl. Lko mouse generation. **b**, Ffar4 expression in major tissues (n = 6). $p < 0.0001$, 95% Confidence Interval = (− 1.031, −0.6134). **c**, Dietary selection assay with HSD/ND in mice (n = 10). **d**, Two bottle preference assay with sucrose (100 mM) in mice (n = 10). **e**, Two bottle preference assay with fructose (100 mM) in mice (n = 10). **f**, Two bottle preference assay with glucose (100 mM) in mice (n = 10). **g**, Two bottle preference assay with dextrin (2%) in mice (n = 10). **h**, Two bottle preference assay with aspartame (0.2%) in mice (n = 10). **i**, Two bottle preference assay with saccharin (0.2%) in mice (n = 10). **j**, Two bottle preference assay with quinine (1.5 mM) in mice (n = 10). **k**, We constructed microglia-specific knockout mice (cx3cr1-CreER; Ffar4Loxp/Loxp, abbreviated Mko), corresponding control mice (Ffar4Loxp/Loxp) are abbreviated as fl/fl. Mko mouse generation. **l**, Ffar4 expression in major tissues (n = 6). $p < 0.0001$, 95% Confidence Interval = (− 1.049, −0.6071). **m**, Dietary selection assay with HSD/ND in mice (n = 10). **n**, Two bottle preference assay with sucrose (100 mM) in mice (n = 10). **o**, Two bottle preference assay with fructose (100 mM) in mice (n = 10). **p**, Two bottle preference assay with glucose (100 mM) in mice (n = 10). **q**, Two bottle preference assay with dextrin (2%) in mice (n = 10). **r**, Two bottle preference assay with aspartame (0.2%) in mice (n = 10). **s**, Two bottle preference assay with saccharin (0.2%) in mice (n = 10). **t**, Two bottle preference assay with quinine (1.5 mM) in mice (n = 10). p values were determined using unpaired, two-tailed t test. Data represent as mean ± SEM. Data shown as a 'box and whiskers' plot; the box extends from the 25th to 75th percentiles, and whiskers with minimum to maximum showing all data points, and the center is median. *$p < 0.05$, **$p < 0.01$, *** $p < 0.001$, ****$p < 0.0001$.

https://doi.org/10.1038/s41564-024-01902-8

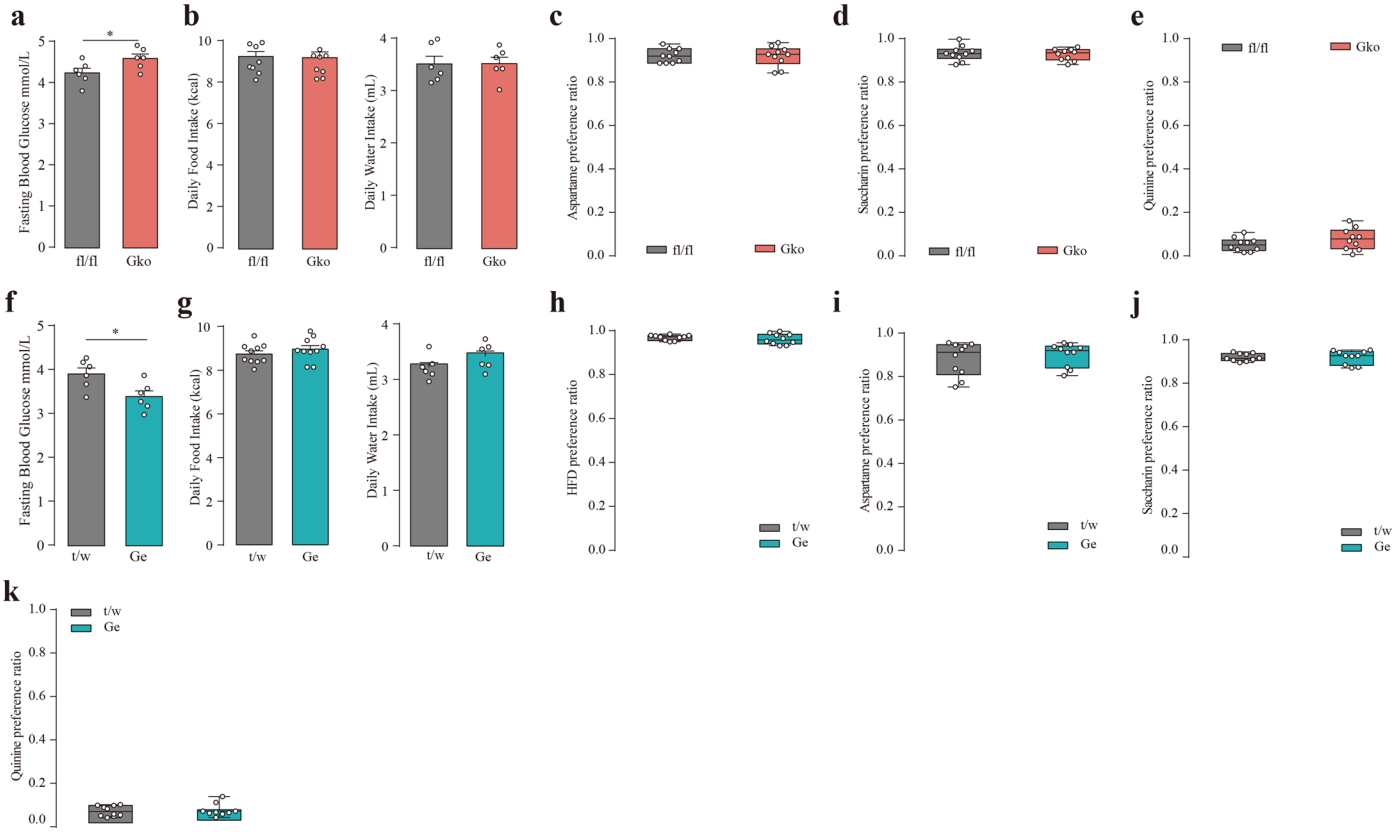

Extended Data Fig. 3 | Ffar4 in the intestine negatively regulates dietary sugar preference. a, Fasting blood glucose levels of mice (n = 6). p = 0.0451, 95% Confidence Interval = (0.009244, 0.6908). **b**, Daily food intake of mice (n = 10) and daily water intake of mice (n = 6). **c**, Two bottle preference assay with aspartame (0.2%) in mice (n = 10). **d**, Two bottle preference assay with saccharin (0.2%) in mice (n = 10). **e**, Two bottle preference assay with quinine (1.5 mM) in mice (n = 10). **f**, Fasting blood glucose levels of Ge mice (n = 6). p = 0.0215, 95% Confidence Interval = (− 0.9397, −0.9358). **g**, Daily food intake of mice (n = 10) and daily water intake of mice (n = 6). **h**, Dietary selection assay with HFD/ND in mice (n = 10). **i**, Two bottle preference assay with aspartame (0.2%) in mice (n = 10). **j**, Two bottle preference assay with saccharin (0.2%) in mice (n = 10). **k**, Two bottle preference assay with quinine (1.5 mM) in mice (n = 10). p values were determined using unpaired, two-tailed t test. Data represent as mean ± SEM. Data shown as a 'box and whiskers' plot; the box extends from the 25th to 75th percentiles, and whiskers with minimum to maximum showing all data points, and the center is median. *p < 0.05, **p < 0.01, *** p < 0.001, ****p < 0.0001.

https://doi.org/10.1038/s41564-024-01902-8

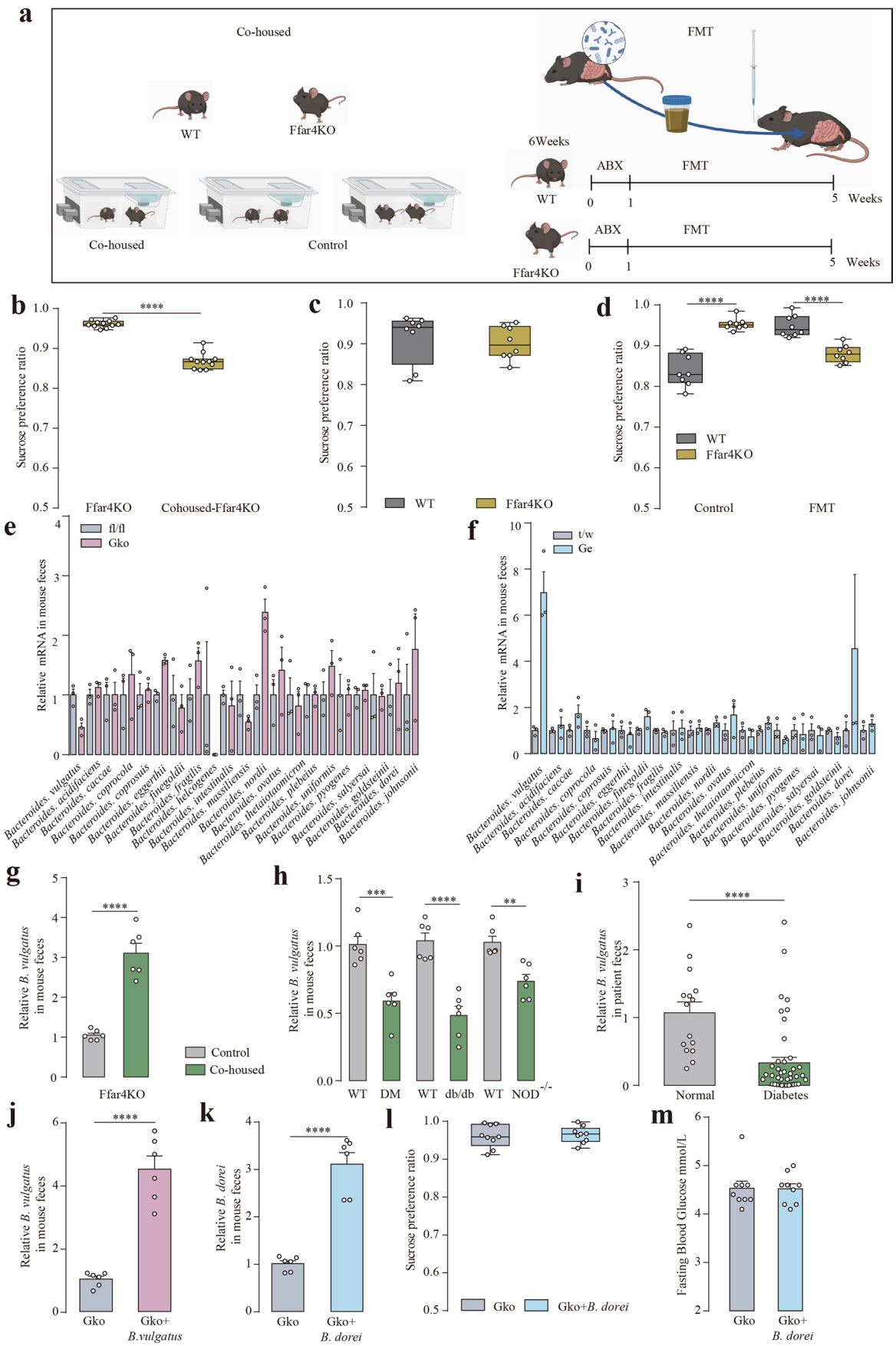

Extended Data Fig. 4 | See next page for caption.

https://doi.org/10.1038/s41564-024-01902-8

Extended Data Fig. 4 | Co-housed/FMT test and quantification of specific bacteria. a, Schematic diagram of co-housed and FMT in Ffar4KO mice and WT mice. **b**, Two bottle preference assay with sucrose (100 mM) in co-housed mice (n = 11). $p < 0.0001$, 95% Confidence Interval = (− 0.1068, −0.07891). **c**, Two bottle preference assay with sucrose (100 mM) in mice administered ABX (n = 8). **d**, Two bottle preference assay with sucrose (100 mM) in mice after FMT (n = 8). $p < 0.0001$, 95% Confidence Interval = (0.08219, 0.1461); $p < 0.0001$, 95% Confidence Interval = (− 0.09394, −0.04260). **e**, Abundance of major strains of Bacteroides in the faeces of Gko mice (n = 3). **f**, Abundance of major strains of Bacteroides in the feces of Ge mice (n = 3). **g**, Quantify of B. vulgatus in Ffar4KO feces after co-housed (n = 6). $p < 0.0001$, 95% Confidence Interval = (1.500, 2.617). **h**, Quantify of B. vulgatus in diabetic mice feces (n = 6). $p = 0.0007$, 95% Confidence Interval = (− 0.6113, −0.2274); $p < 0.0001$, 95% Confidence Interval = (− 0.7507, −0.3570); $p = 0.0022$. **i**, Quantify of B. vulgatus in feces from healthy controls and diabetic patients (n = 15/45). $p < 0.0001$. **j**, Localization in mice after B. vulgatus back-supplementation (n = 6). $p < 0.0001$, 95% Confidence Interval = (2.448, 4.318). **k**, Localization in mice after B. dorei back-supplementation (n = 6). $p < 0.0001$, 95% Confidence Interval = (1.526, 2.629). **l**, Two bottle preference assay with sucrose (100 mM) in Gko mice after back-supplementation with B. dorei (n = 9). **m**, Fasting blood glucose levels after back-supplementation with B. dorei (n = 9). p values were determined using unpaired, two-tailed t test. Data represent as mean ± SEM. Data shown as a 'box and whiskers' plot; the box extends from the 25th to 75th percentiles, and whiskers with minimum to maximum showing all data points, and the center is median. *$p < 0.05$, **$p < 0.01$, *** $p < 0.001$, ****$p < 0.0001$.

https://doi.org/10.1038/s41564-024-01902-8

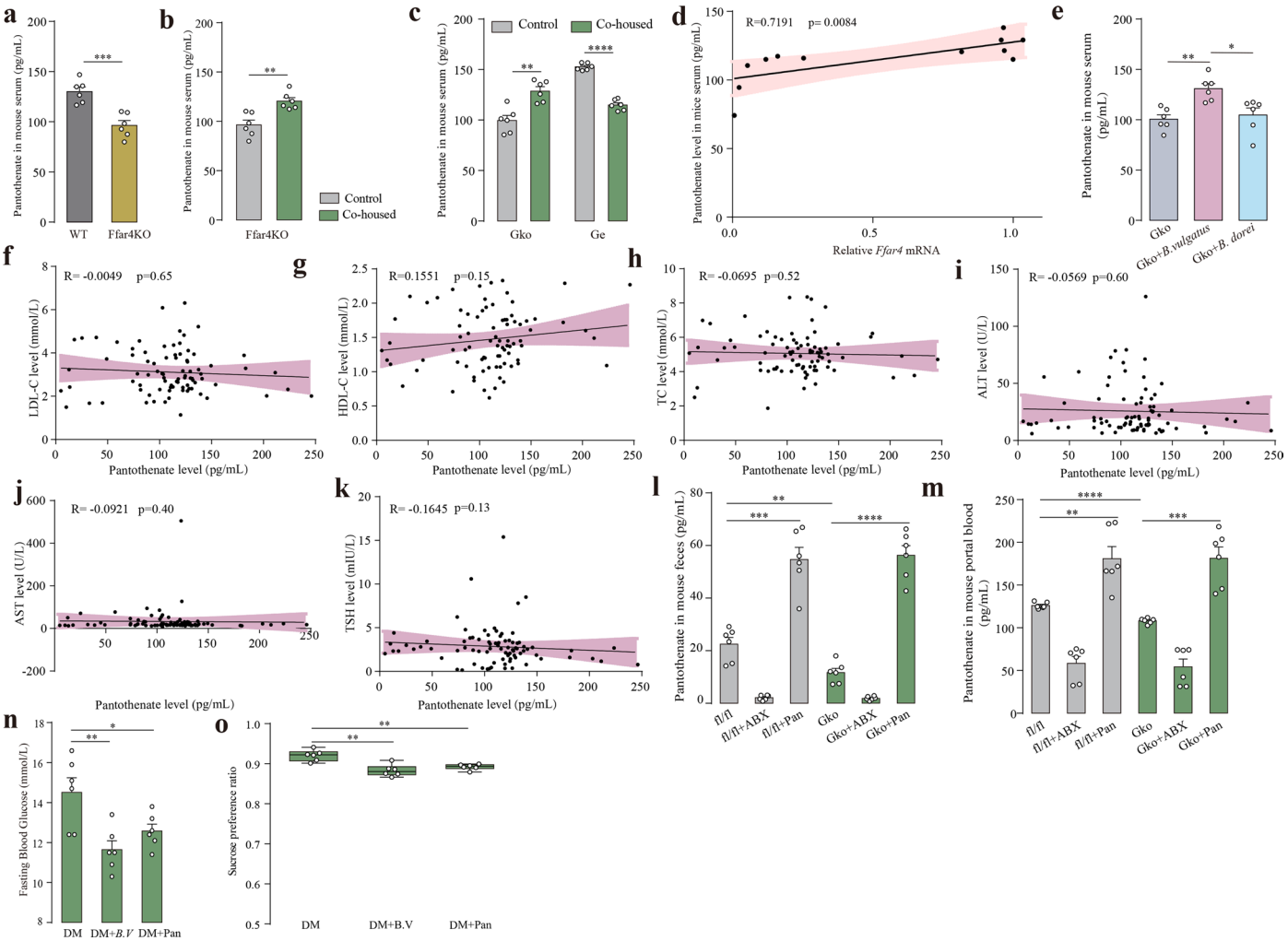

Extended Data Fig. 5 | Correlation between serum pantothenate levels and biochemical indices. a, Pantothenate levels in Ffar4KO serum (n = 6). p = 0.0006, 95% Confidence Interval = (− 48.77, −18.60). **b**, Pantothenate levels in Ffar4KO serum after co-housed (n = 6). p = 0.0005, 95% Confidence Interval = (11.59, 29.98). **c**, Pantothenate levels in Gko or Ge serum after co-housed (n = 6). p = 0.0012, 95% Confidence Interval = (14.55, 43.79); p < 0.0001, 95% Confidence Interval = (− 43.45, −31.95). **d**, The correlation between Ffar4 mRNA levels in gut and pantothenate levels in mouse serum (n = 12). **e**, Assay of pantothenate levels in mouse serum after back-supplementation with B. vulgatus or B. dorei (n = 6). p = 0.0011, 95% Confidence Interval = (15.42, 45.29); p = 0.0122, 95% Confidence Interval = (− 45.37, −7.070) **f-k**, The correlation between pantothenate levels in patient serum and LDL/HDL/TC/ALT/AST/TSH levels in patient serum (n = 24/36). **l**, Pantothenate levels in mouse feces (n = 6). p = 0.0001, 95% Confidence Interval = (20.49, 44.00); p = 0.0055, 95% Confidence Interval = (− 17.63, −3.970); p < 0.0001, 95% Confidence Interval = (35.63, 53.58). **m**, Pantothenate levels in mouse portal blood (n = 6). p = 0.0033, 95% Confidence Interval = (23.00, 86.50); p < 0.0001, 95% Confidence Interval = (− 22.35, −13.46); p = 0.0002, 95% Confidence Interval = (43.98, 102.7). **n**, Fasting blood glucose levels in diabetic mice after back-supplementation with B. vulgatus and pantothenate (n = 6). p = 0.0069, 95% Confidence Interval = (− 4.753, −0.9803); p = 0.0359, 95% Confidence Interval = (− 3.712, −0.1547). **o**, Two bottle preference assay with sucrose (100 mM) in diabetic mice after back-supplementation with B. vulgatus and pantothenate (n = 6). p = 0.0011, 95% Confidence Interval = (− 0.05573, −0.01883); p = 0.0013, 95% Confidence Interval = (− 0.04242, −0.01405). p values were determined using unpaired, two-tailed t test. Data represent as mean ± SEM. Data shown as a 'box and whiskers' plot; the box extends from the 25th to 75th percentiles, and whiskers with minimum to maximum showing all data points, and the center is median.*p < 0.05, **p < 0.01, *** p < 0.001, ****p < 0.0001.

https://doi.org/10.1038/s41564-024-01902-8

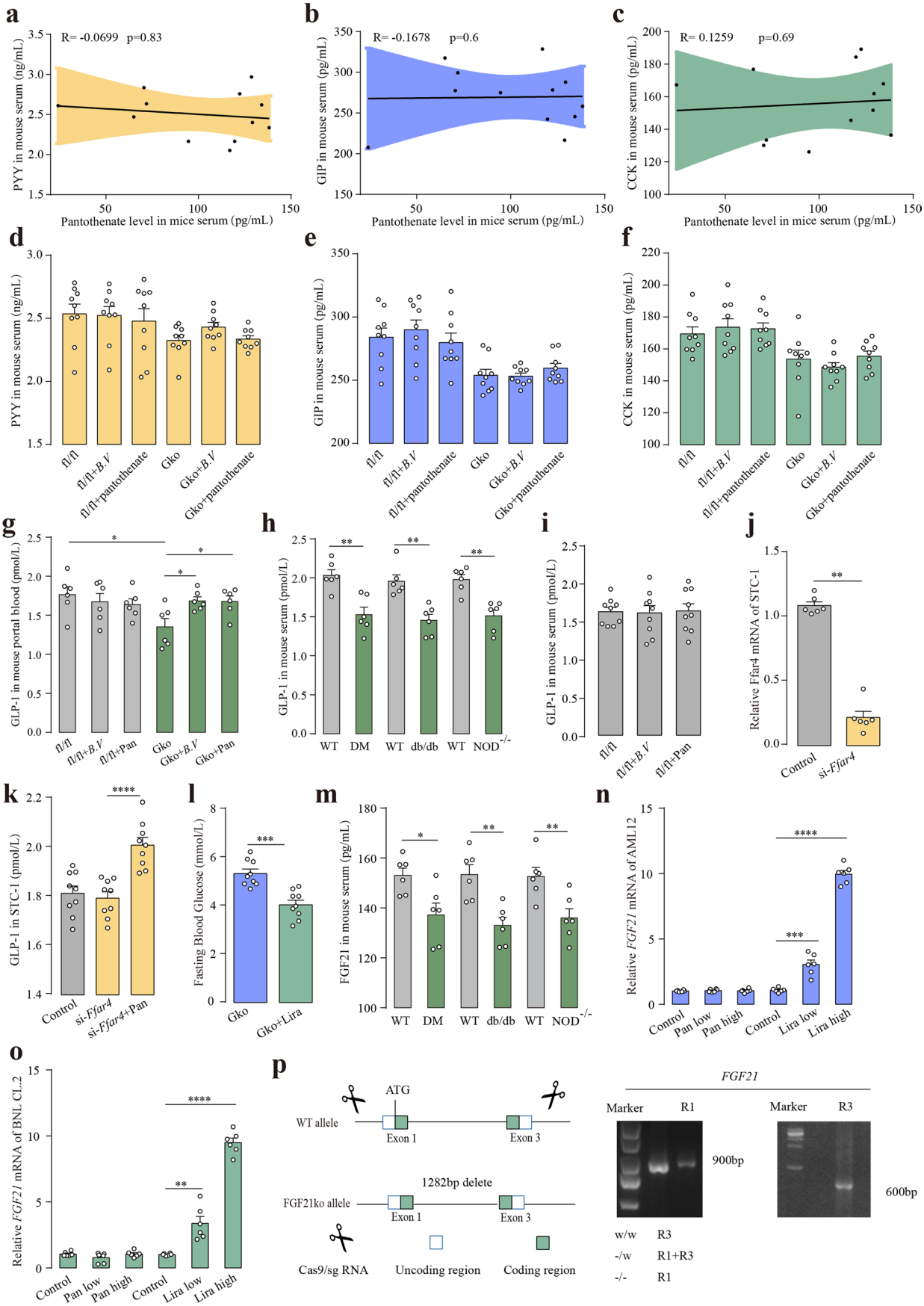

Extended Data Fig. 6 | See next page for caption.

https://doi.org/10.1038/s41564-024-01902-8

Extended Data Fig. 6 | GLP-1-FGF21 axis is a key downstream regulator of Ffar4-B. vulgatus-pantothenate. a-c, The correlation between pantothenate levels in mouse serum and PYY/GIP/CCK levels in mouse serum (n = 6). **d-f**, Assay of PYY/GIP/CCK contents in mouse serum (n = 9). **g**, Assay of GLP-1 content in mouse portal blood (n = 6). p = 0.0183, 95% Confidence Interval = (− 0.7389, −0.008591); p = 0.0173, 95% Confidence Interval = (0.07245, 0.5931); p = 0.0279, 95% Confidence Interval = (0.04308, 0.6056). **h**, Assay of GLP-1 content in diabetic mice serum (n = 6). p = 0.0018, 95% Confidence Interval = (− 0.7705, −0.2362); p = 0.0012, 95% Confidence Interval = (− 0.7526, −0.2501); p = 0.0022. **i**, Assay of GLP-1 content in mouse serum (n = 9). **j**, Ffar4 expression after knockdown of Ffar4 in STC-1 cells (n = 6). p = 0.0022. **k**, Assay of GLP-1 content in STC-1 cells (n = 9). p < 0.0001, 95% Confidence Interval = (0.1231, 0.2858). **l**, Fasting blood glucose levels (n = 9). p = 0.0001, 95% Confidence Interval = (− 1.809, −0.7240). **m**, Assay of FGF21 content in diabetic mice serum (n = 6). p = 0.0176, 95% Confidence Interval = (− 28.18, −3.396); p = 0.0024, 95% Confidence Interval = (− 31.61, −9.116); p = 0.0093, 95% Confidence Interval = (− 28.14, −5.087). **n-o**, FGF21 gene expression in AML-12/BNL CL. 2 cells after treatment with pantothenate/liraglutide (n = 6). p = 0.0002, 95% Confidence Interval = (1.212, 2.728); p < 0.0001, 95% Confidence Interval = (8.202, 9.542); p = 0.0010, 95% Confidence Interval = (1.207, 3.516); p < 0.0001, 95% Confidence Interval = (7.673, 9.256). **p**, FGF21KO mouse generation. Genotyping primers amplified a 600-bp band from wild-type mouse DNA and a 900-bp band from FGF21KO mouse DNA (n = 6). p values were determined using unpaired, two-tailed t test. Data represent as mean ± SEM. *p < 0.05, **p < 0.01, *** p < 0.001, ****p < 0.0001.

https://doi.org/10.1038/s41564-024-01902-8

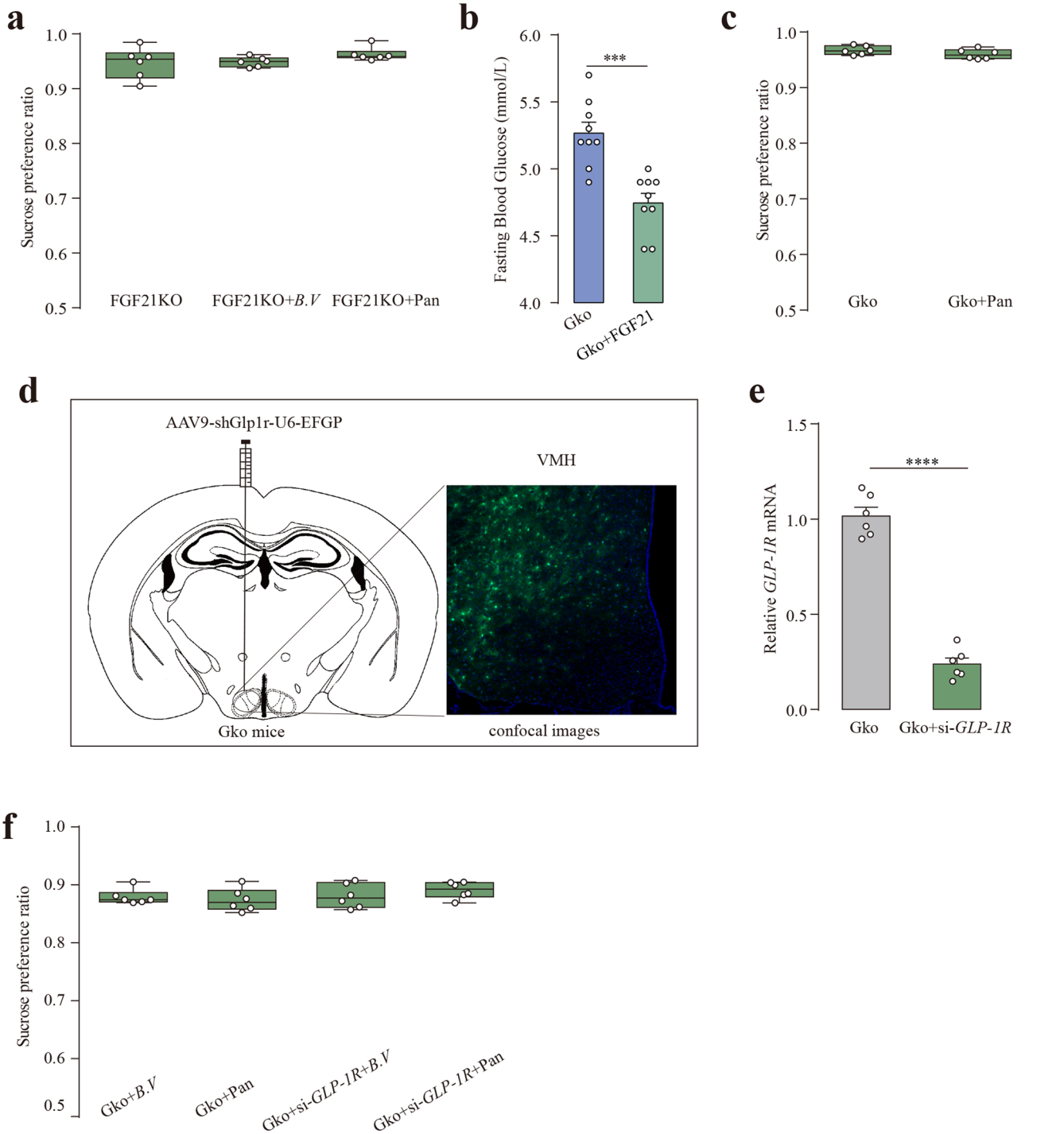

Extended Data Fig. 7 | Sugar preference does not change in mice after silenced VHM GLP-1R. a, Two bottle preference assay with sucrose (100 mM) in FGF21KO after back-supplementation with B. vulgatus and pantothenate (n = 6). **b**, Fasting blood glucose levels (n = 9). p = 0.0003, 95% Confidence Interval = (− 0.7756, −0.2911). **c**, Two bottle preference assay with sucrose (100 mM) in Gko after Stereotaxic injection with pantothenate (n = 6). **d**, Inject AAV9-shGlp1r-U6-EFGP into the VMH of Gko mice and image the brain sections. **e**, GLP-1R expression in VMH of Gko mice (n = 6). p < 0.0001, 95% Confidence Interval = (− 0.9013, −0.6548). **f**, Two bottle preference assay with sucrose (100 mM) in Gko after back-supplementation with B. vulgatus and pantothenate (n = 6). p values were determined using unpaired, two-tailed t test. Data represent as mean ± SEM. Data shown as a 'box and whiskers' plot; the box extends from the 25th to 75th percentiles, and whiskers with minimum to maximum showing all data points, and the center is median. *p < 0.05, **p < 0.01, *** p < 0.001, ****p < 0.0001.

https://doi.org/10.1038/s41564-024-01902-8

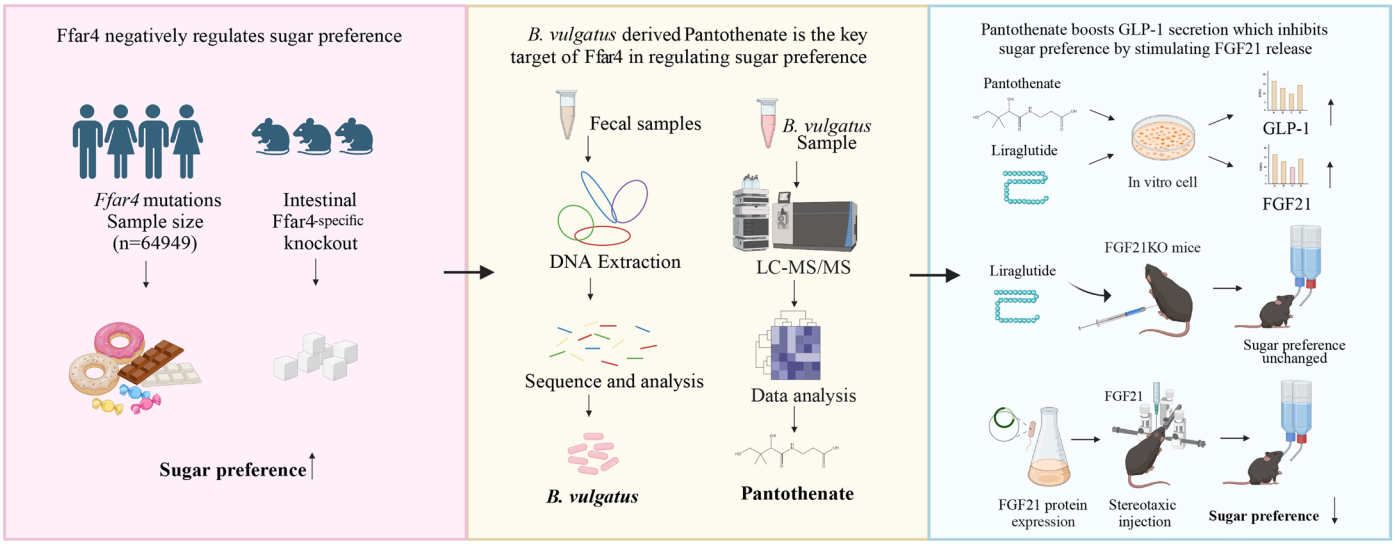

Extended Data Fig. 8 | Graphical summary of results. Ffar4 deficiency or inactivation increases the host's sugar preference. Knockout of Ffar4 in intestinal epithelial cells leads to changes in gut microbiota which decrease in B. vulgatus abundance. The metabolite pantothenate of B. vulgatus stimulates the secretion of GLP-1 in enteroendocrine cells. GLP-1 stimulates an increase in FGF21 secretion, which enters the blood-brain barrier and acts on neurons in the VMH, altering sugar preferences.

nature portfolio

Corresponding author(s): Shenglong Zhu

Last updated by author(s): Feb 14, 2024

Reporting Summary

Nature Portfolio wishes to improve the reproducibility of the work that we publish. This form provides structure for consistency and transparency in reporting. For further information on Nature Portfolio policies, see our Editorial Policies and the Editorial Policy Checklist.

Statistics

For all statistical analyses, confirm that the following items are present in the figure legend, table legend, main text, or Methods section.

n/a	Confirmed	
☐	☒	The exact sample size (*n*) for each experimental group/condition, given as a discrete number and unit of measurement
☐	☒	A statement on whether measurements were taken from distinct samples or whether the same sample was measured repeatedly
☐	☒	The statistical test(s) used AND whether they are one- or two-sided *Only common tests should be described solely by name; describe more complex techniques in the Methods section.*
☒	☐	A description of all covariates tested
☐	☒	A description of any assumptions or corrections, such as tests of normality and adjustment for multiple comparisons
☐	☒	A full description of the statistical parameters including central tendency (e.g. means) or other basic estimates (e.g. regression coefficient) AND variation (e.g. standard deviation) or associated estimates of uncertainty (e.g. confidence intervals)
☐	☒	For null hypothesis testing, the test statistic (e.g. *F*, *t*, *r*) with confidence intervals, effect sizes, degrees of freedom and *P* value noted *Give P values as exact values whenever suitable.*
☒	☐	For Bayesian analysis, information on the choice of priors and Markov chain Monte Carlo settings
☒	☐	For hierarchical and complex designs, identification of the appropriate level for tests and full reporting of outcomes
☒	☐	Estimates of effect sizes (e.g. Cohen's *d*, Pearson's *r*), indicating how they were calculated

Our web collection on statistics for biologists contains articles on many of the points above.

Software and code

Policy information about availability of computer code

Data collection	LC-MS/MS analysis was performed using an UHPLC (1290 Infinity LC, Agilent Technologies) coupled to a quadrupole time-of-flight (AB Sciex TripleTOF 6600); 16S rRNA gene sequencing was performed using an Illumina MiSeq/Novaseq(Illumina, San Diego, CA, USA)
Data analysis	GraphPad Prism V9 were used to basic statistical analysis and generate graphs; Western Blot protein band intensity quantification was performed by Image (version 1.52a); 16S rRNA gene sequencing analysis: Cutadapt 1.9.1, Vsearch 1.9.6, Qiime 1.9.1, RDP Classifier 2.2, PyNAST 1.2, R 3.3.1, LEfSe 1.0, PICRUSt 1.0, KronaTools 2.7, Cytoscape 3.5.1, GraPhlAn 1.0, and Circos 0.69-1. LC-MS/MS analysis:The raw MS data were converted to MzXML files using ProteoWizard MSConvert before importing into freely available XCMS 4.4.0.

For manuscripts utilizing custom algorithms or software that are central to the research but not yet described in published literature, software must be made available to editors and reviewers. We strongly encourage code deposition in a community repository (e.g. GitHub). See the Nature Portfolio guidelines for submitting code & software for further information.

Data

Policy information about availability of data

All manuscripts must include a data availability statement. This statement should provide the following information, where applicable:

- Accession codes, unique identifiers, or web links for publicly available datasets
- A description of any restrictions on data availability
- For clinical datasets or third party data, please ensure that the statement adheres to our policy

All 16S rRNA gene amplicon sequencing data were deposited at the NCBI under the accession code PRJNA1186342. The metabolomics data were deposited in the MetaboLights MTBLS11684. All data are available in the main text, extended data or supplementary materials. Source data are provided with this paper.

Research involving human participants, their data, or biological material

Policy information about studies with human participants or human data. See also policy information about sex, gender (identity/presentation), and sexual orientation and race, ethnicity and racism.

Reporting on sex and gender	Neither biological sex or gender was considered when designing or consenting participants for this study.
Reporting on race, ethnicity, or other socially relevant groupings	Race and ethnicity were not considered when is study.
Population characteristics	The population characteristics are reported in Supplementary Table 2-3.
Recruitment	The peripheral blood samples from a total of 60 individuals with type 2 diabetes and from 24 healthy controls were recruited from Jiangnan University Medical Center. All the participants with type 2 diabetes met the diagnostic criteria established by the American Diabetes Association. Prior to their inclusion in the study, all the participants or their legal guardians provided written informed consent. The samples were collected from a health examination center of hospital with no restriction on gender, ensuring that there is no selection bias.
Ethics oversight	The Medical Ethics Committee of Jiangnan University (Ref. No. JNU20210310IRB01) and Medical Ethics Review Approval Document of Wuxi Second People's Hospital (2024-Y-156) approved the collection of peripheral blood from both diabetes patients and healthy donors.

Note that full information on the approval of the study protocol must also be provided in the manuscript.

Field-specific reporting

Please select the one below that is the best fit for your research. If you are not sure, read the appropriate sections before making your selection.

☒ Life sciences ☐ Behavioural & social sciences ☐ Ecological, evolutionary & environmental sciences

For a reference copy of the document with all sections, see nature.com/documents/nr-reporting-summary-flat.pdf

Life sciences study design

All studies must disclose on these points even when the disclosure is negative.

Sample size	Sample size was chosen according to institutional directives and in accordance with the 3Rs rules guiding principles underpinning the humane use of animals in research, but no statistical methods were used to predetermine sample size.But our sample sizes are similar to previous reports.
Data exclusions	No data were excluded from this study.
Replication	All the main findings were repeated by at least 3 independent experiments. All attempts for replication were successful.
Randomization	Human studies was an observational study, so subjects were not randomized. For the animal and in vitro cultures,we randomly allocated at the beginning of each experiments.
Blinding	As this was not a clinical tria, blinding was not relevant. Analyses were conducted in a manner blinded to the experimenter.

Reporting for specific materials, systems and methods

We require information from authors about some types of materials, experimental systems and methods used in many studies. Here, indicate whether each material, system or method listed is relevant to your study. If you are not sure if a list item applies to your research, read the appropriate section before selecting a response.

Materials & experimental systems

n/a	Involved in the study
☐	☒ Antibodies
☐	☒ Eukaryotic cell lines
☒	☐ Palaeontology and archaeology
☐	☒ Animals and other organisms
☒	☐ Clinical data
☒	☐ Dual use research of concern
☒	☐ Plants

Methods

n/a	Involved in the study
☒	☐ ChIP-seq
☒	☐ Flow cytometry
☒	☐ MRI-based neuroimaging

Antibodies

Antibodies used	FGF21 Rabbit mAb (Abclonal,CAT# A3908, 1:1000,CloneID ARC53983); β-Actin Rabbit mAb (Abclonal,CAT# AC026, 1:1000,CloneID ARC5115-01); HRP-conjugated Goat Anti-Mouse IgG H&L (Biodragon, CAT# BF03009,1:5000)
Validation	All antibodies are obtained from commercial sources, and vendors have shown validation on their websites.

Eukaryotic cell lines

Policy information about cell lines and Sex and Gender in Research

Cell line source(s)	STC-1 cells, AML12 cells, and BNL CL.2 cells were obtained from the National Collection of Authenticated Cell Cultures.
Authentication	The cell lines were bought from National Collection of Authenticated Cell Cultures with authentication (STR profiling)
Mycoplasma contamination	The cell lines were not detected for mycoplasma contamination.
Commonly misidentified lines (See ICLAC register)	No commonly misidentified cell lines were used.

Animals and other research organisms

Policy information about studies involving animals; ARRIVE guidelines recommended for reporting animal research, and Sex and Gender in Research

Laboratory animals	Description of research mice used for experiments can be found in the relevant figure legends and Methods.The total Ffar4-knockout (KO, RRID: MGI: 7256540) mice, Villin-Cre mice, and Alb-Cre mice were obtained from Shanghai Bioraylab and Shanghai Biomodel Organism. Floxed FFAR4 (fl/fl, RRID: MGI: 7256541) and FFAR4 transgenic (t/w, RRID: MGI: 7256542) mice were constructed commercially by Shanghai Biomodel Organism and Nanjing Biomedical Research Institute of Nanjing University, respectively. Total FGF21-knockout (strain no. T012638), db/db, and db/m mice were purchased from GemPharmatech (Nanjing, China).
Wild animals	No wild animals were involved in this study.
Reporting on sex	Only male mice were used in this study.
Field-collected samples	No field-collected samples were involved in this study.
Ethics oversight	All the animal procedures adhered to the Guide for Care and Use of Laboratory Animals of the School of Medicine, Jiangnan University, and were approved by the Animal Ethics Committee of Jiangnan University (JN No:20200515t0030810).

Note that full information on the approval of the study protocol must also be provided in the manuscript.

Plants

Seed stocks	*Report on the source of all seed stocks or other plant material used. If applicable, state the seed stock centre and catalogue number. If plant specimens were collected from the field, describe the collection location, date and sampling procedures.*
Novel plant genotypes	*Describe the methods by which all novel plant genotypes were produced. This includes those generated by transgenic approaches, gene editing, chemical/radiation-based mutagenesis and hybridization. For transgenic lines, describe the transformation method, the number of independent lines analyzed and the generation upon which experiments were performed. For gene-edited lines, describe the editor used, the endogenous sequence targeted for editing, the targeting guide RNA sequence (if applicable) and how the editor was applied.*
Authentication	*Describe any authentication procedures for each seed stock used or novel genotype generated. Describe any experiments used to assess the effect of a mutation and, where applicable, how potential secondary effects (e.g. second site T-DNA insertions, mosiacism, off-target gene editing) were examined.*